Front. Chem. Sci. Eng. 2021, 15(6): 1380–1407
https://doi.org/10.1007/s11705-021-2097-z

REVIEW ARTICLE

Hollow carbon spheres and their noble metal-free hybrids in catalysis

Xiang-Hui Yu[1], Jin-Long Yi[1], Ru-Liang Zhang[1], Feng-Yun Wang[2], Lei Liu (✉)[1]

1 School of Materials Science and Engineering, Shandong University of Science and Technology, Qingdao 266590, China
2 College of Physics and State Key Laboratory of Bio Fibers and Eco Textiles, Qingdao University, Qingdao 266071, China

Abstract Hollow carbon spheres have garnered great interest owing to their high surface area, large surface-to-volume ratio and reduced transmission lengths. Herein, we overview hollow carbon sphere-based materials and their noble metal-free hybrids in catalysis. Firstly, we summarize the key fabrication techniques for various kinds of hollow carbon spheres, with a particular emphasis on controlling pore structure and surface morphology, and then heterogeneous doping as well as their metal-free/containing hybrids are presented; next, possible applications for non-noble metal/hollow carbon sphere hybrids in the area of energy-related catalysis, including oxygen reduction reaction, hydrogen evolution reaction, oxygen evolution reaction, water splitting, rechargeable Zn-air batteries and pollutant degradation are discussed; finally, we introduce the various challenges and opportunities offered by hollow carbon spheres from the perspective of synthesis and catalysis.

Keywords hollow carbon spheres, functionalization, noble metal-free, catalysis

1 Introduction

Among carbon materials, hollow-structured carbon materials possess a unique architecture with various advantageous features, including having a high surface area, a spherical structure with interior cavity, low density, and a shortened transmission distance. Consequently, hollow carbon spheres (HCSs) have garnered great interest from researchers for their potential application in energy storage, catalysis support, adsorbents and so on [1–4].

In past decades, many attempts have been made to achieve the controllable synthesis and functionalization of HCSs with the aim to create advanced nanostructures. Though preparation methods for HCSs have been studied for a long time, they are yet to be perfected. Developments in synthesis methods have enriched the nanostructure, chemical properties and morphology of HCSs. Fabrication of HCSs through templating, template-free and self-template methods, mean plentiful variations in structural complexity, such as diameters that range from nano- to microscale, diverse morphologies, tunable porosities and diverse shell constituents [5–7].

The functionalization of HCSs has been widely investigated with the incorporation of heteroatoms and/or metal/metal-free content. Their morphologies, surface chemistry and composition can be flexibly regulated for use as electrodes in supercapacitors, Li-S batteries, metal-air batteries and photocatalysts [8–10]. Their porous shell can serve as a carrier for the adsorption/transmission/reaction of guest species [11–16]. Moreover, considering their operating environment (acid or base), their high chemical stability is particularly important. Several recently published reviews have summarized the progress of the on-going research into hollow-structured carbon materials [17–20], which mainly focus on preparation techniques, various nanostructures, and applications in the energy storage field. The structure control, functionalization and catalysis performances of HCSs on the other hand were not included in these studies.

Based on this point, we herein give an overview of HCSs-based materials and their non-noble metal-based hybrids for catalysis. Firstly, we summarize the synthesis strategies of various kinds of HCSs by means of hard-templating, soft-templating, and template-free/self-template methods; next, we present surface morphology and pore structure control methods, heterogeneous doping, as well as their metal-free/containing hybrids; in the third part, we highlight the applications of non-precious metal/HCSs hybrids in the area of energy-related catalysis; in the

Received April 24, 2021; accepted July 19, 2021

E-mail: liulei@sdust.edu.cn

final part, we present a brief discussion and explore further possible directions for HCSs-based materials.

2 Synthesis and functionalization

Tremendous endeavors have been undertaken to design and construct the nanostructures of HCSs. In this paper, the different synthesis approaches, including hard- and soft-templating, self-templating and template-free methods, are employed to control the morphologies and porous structures present in the shells of HCSs. Furthermore, the surface chemistry and incorporated guest species are considered important factors governing the HCSs' properties. The functionalization of HCSs is presented in terms of heteroatom doping, HCSs/carbon hybrids and HCSs/metal-based hybrids.

2.1 Preparation method

2.1.1 Hard-templating

Hard-templating is the most common approach for HCS fabrication, and contains several steps. Firstly, monodispersed templates of a certain size are prepared; secondly, a preselected carbon precursor is layer-coated onto the spherical templates so as to construct a core-shell structure; finally, HCSs are fabricated following high temperature pyrolysis and template removal.

Monodispersed colloidal spheres, such as SiO_2 spheres, polymer spheres, and metallic powder, are employed as the hard core due to their ease of fabrication [21,22]. The carbon precursors, including resorcinol-formaldehyde (RF) resin, dopamine, glucose, metal-organic framework, and conducting polymers [23–25], can be adsorbed on the colloidal templates surface through Van der Waals force or electrostatic adsorption. Owing to the hard template's advantages of uniformity and monodispersity, the fabricated HCSs from this method usually possess a narrow particle size distribution and well-controlled morphology.

Benefiting from their low cost and controllable particle size, ranging from nano- to micro-scale, SiO_2 spheres are the most widely-used templates for the synthesis of spherical hollow structures. SiO_2 cores can be etched away through treatment with hydrofluoric acid or NaOH, thereby finally leaving carbonaceous shell. An instance of this was shown by Fan et al. [26], who derived HCSs from core-shell structured SiO_2@phenolic resin/SiO_2 spheres through a two sol-gel process. In order to enhance the interaction of negatively charged RF resin and SiO_2 spheres, surfactants, such as cetyltrimethylammonium bromide [27] or polyvinylpyrrolidone [28], were used to modify the SiO_2 surface to a positive charge. Following this, electrostatic interaction was used to promote the RF resin coating process onto the SiO_2 sphere. Repeating the coating process can further control the HCS shell structure. This was shown by Bu et al. [29], who fabricated double shell HCSs through a multiple coating approach. As shown in Fig. 1, SiO_2 spheres were first covered by polydopamine (PDA) (denoted as SiO_2@PDA), subsequently another SiO_2 layer was coated on the SiO_2@PDA surface with the aid of polyvinylpyrrolidone, and finally SiO_2@PDA@-SiO_2@PDA composites were obtained following another coating of PDA (Fig. 1(a)). Transmission electron microscope (TEM) images show that the HCSs can be controlled either in single shell (SHCS) or double shell (DHCS). By tuning the mass ratio of SiO_2 to dopamine, the thicknesses of the PDA layers can be modulated in the range of 45–100 nm (Figs. 1(b–e)).

Polymer-based templates, such as polystyrene spheres, poly(methyl methacrylate) (PMMA) spheres, and melamine-formaldehyde (MF) nanospheres, are also attracting increased attention in their role as templates. When compared with SiO_2, removing polymer-based templates is a milder process. They can be removed through carbonization or dissolution [30,31]. Taking advantage of PMMA's ability to completely decompose in temperatures over 400 °C, Yang et al. [32] used an *in-situ* polymerization method to coat RF on its surface. Carbonization realized the decomposition of PMMA and transformed the RF resin to carbon shell. HCSs with a diameter of 400–1000 nm were obtained. The key to polymer spheres removal by dissolution is to select a carbon precursor that is insoluble in the given organic solvent. He et al. [33] designed N-doped HCSs (NHCSs) by preparing ZIF-8 shell on the surface of the polystyrene microspheres, wherein polystyrene was selectively removed by *N*,*N*-dimethylformamide.

As another kind of polymer, MF nanospheres are superior to both polystyrene spheres and PMMA spheres, owing to their N-containing characteristic. The released N-containing gases during the carbonization process can activate the carbon shell and introduce N into the carbon skeleton. All these merits make it an ideal template for NHCSs fabrication, with this method being named "one-pot carbonization". Our group further developed this strategy by coating RF resin onto MF spheres (1.5 μm) [34,35]. Notably, monodispersed NHCSs were fabricated with a particle size of 720 nm and a N content as high as 7.2%.

In addition to the above mentioned hard cores, many other hard templates have also been explored for HCS synthesis, including calcarea carbonica [36,37], biomass [38], as well as metal and metal oxide powder [39,40]. For example, Zhao's groups [36] utilized $CaCO_3$ hollow spheres, and Zhang's group [37] employed spherical $CaCO_3$ as the template and PDA as the carbon source to fabricate HCSs. The use of $CaCO_3$ offers similar advantages to MF spheres through a self-activation mechanism. The released CO_2 from the decomposition of the $CaCO_3$ can activate the carbon shell and introduce abundant pores to achieve a high surface area.

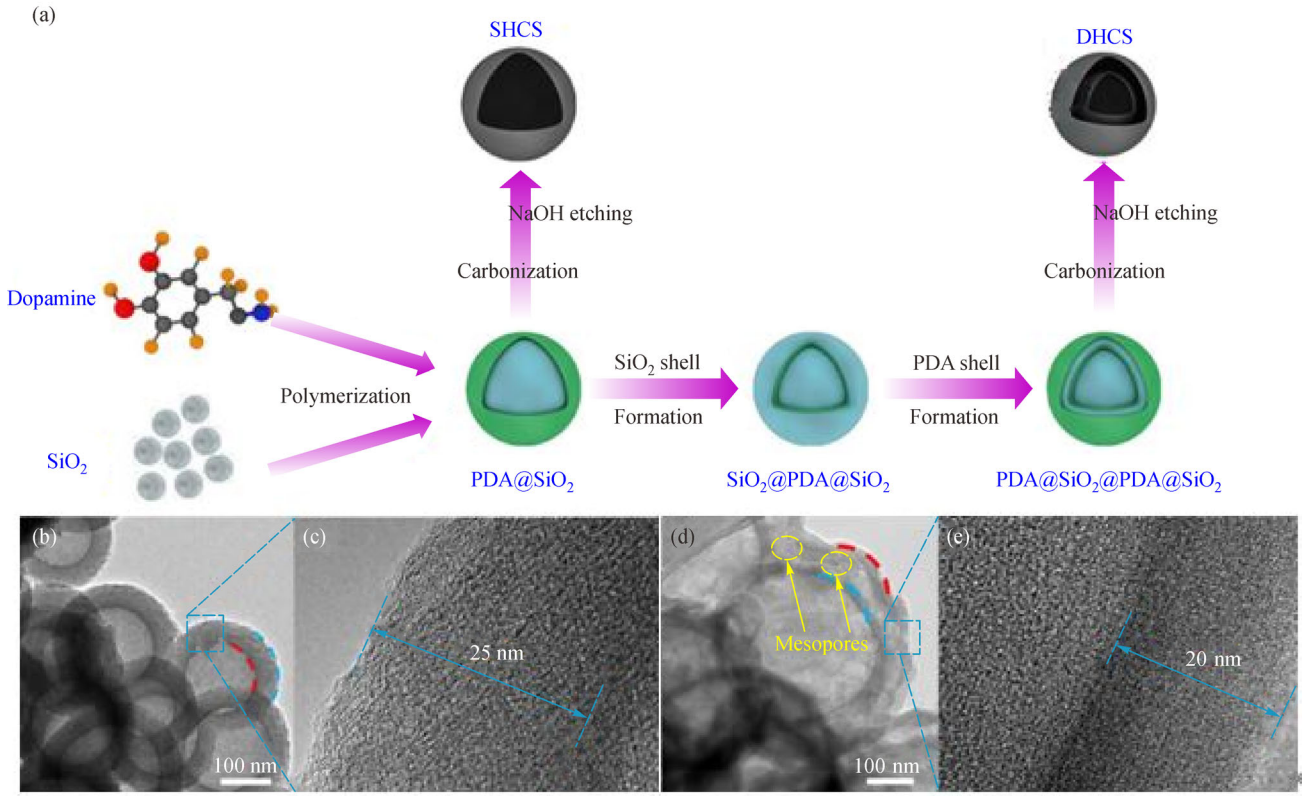

Fig. 1 (a) Schematic illustration of the DHCS and SHCS preparation procedures; (b, d) TEM and (c, e) high resolution TEM (HRTEM) images of the SHCSs and DHCSs. Reprinted with permission from ref. [29], copyright 2021 Elsevier.

2.1.2 Soft templating

The hard-templating method requires a multiple step synthetic procedure. In addition, due to their being exact duplicates, the porous structures and morphologies of the replicated HCSs rely on the original templates. The soft-templating strategy, which on account of the co-assembly of carbon precursors and colloidal systems, and can be carried out with relative easy and convenience, is formed *in-situ* by virtue of the "soft" templates. Additionally, it can be easily removed by pyrolysis or extraction. The "soft" core is usually generated from extensive organic additives or surfactants, such as nanoemulsion droplets [41], micelles [42,43], vesicles [44] or gas bubbles [45].

Soft-templating system containing triblock copolymers (poly(ethylene glycol)-*block*-poly(propylene glycol)-*block*-poly(ethylene glycol)) and anion surfactants (sodium oleate) was coupled with a hydrothermal carbonization of glucose to prepare HCSs. When adjusting the hydrothermal carbonization time, the hollow carbon bowls and capsules exhibited a tunable diameter of 550–600 nm [46]. In addition, polyacrylic acid was employed as an eco-friendly soft template so as to produce hollow cores. This could be easily removed by water without the need for any other chemical reagents [41]. In an interesting study, Liu et al. [47] focused on the interior structure of the HCSs. They used Pickering emulsions as spherical templates to design mesoporous carbon microspheres, within which phenolic resol was used as the carbon precursor, silica as the emulsifier, and F127 as the surfactant. Both outer and interior architectures were independently formed during this process, the details of which are illustrated in Fig. 2. The outer crusts were obtained through spherical Pickering water droplets, while the internal structures were created by assembling F127 and phenolic resol inside the Pickering emulsion. The easily occurring heterogeneous nucleation at the oil/water interfaces favored the polymerization of resol oligomers/F127 composites, and formed a mesostructure around the inner surfaces of the water droplets (Fig. 2(a)). Once the concentration of resol oligomers/F127 composites reached a certain level, homogeneous nucleation started to occur in the inner space (Fig. 2(b)). By adjusting the synthesis parameters, the interior structures were then constructed as hollow, multi-chambered, bijel-structured, multi-cored "solid", or honeycombed. To produce nanoemulsion droplets, Chen et al. [48] utilized volatile oils (e.g., toluene, cyclohexane, isooctane and heptane) as the oil

phase. The usage of organosilane as the carbon source and pore-forming agent was crucial to the formation of HCSs. The hydrolyzation of organosilane could stabilize the oil-in-water emulsion, and form a solidified polysilsesquioxane shell around the oil droplet (Fig. 2(c)). The HCSs were obtained following the oil evaporation, carbonization and etching template in the shell.

2.1.3 Template-free/self-templating method

The template-free/self-templating process avoids the template fabrication and removal processes, meaning that it is more economic, time-saving and convenient than the template procedures. Through this method, HCSs can be obtained through direct carbonization. An example of this was demonstrated by Sun et al. [44], who assembled poly (amic acid) to uniform homopolymer vesicles with a diameter of 200 nm. NHCSs could be easily obtained by pyrolysis the crosslinked construction of poly(amic acid) vesicles and melamine. Microporous hypercrosslinked polymers were also utilized to create hollow microporous carbon spheres with a well-controlled porous structure, hollow voids, and shell thickness [49]. Another method to fabricate HCSs, is through the direct carbonization of ground soybean waste [50], hollow ZIF-8 nanospheres [51] and natural hollow-structured puffball spores [52]. Chen's group found a new method, whereby they took advantage of the different polymerization rate and degree of outer and inner RF resin, and prepared a heterogeneous resin sphere. After using acetone to selectively remove the inner low-molecular-weight RF oligomer, HCSs with different inner structures (hollow and yolk-shell) were created [53].

For a large scale synthesis of the millimeter-sized HCSs, Zhou et al. [54] proposed fabricating hollow polyacrylonitrile and carbon spheres through a phase-separation approach. This method coupled a modified phase-inversion process with a gas-foaming process. As shown in Fig. 3, when a solution containing *N*-dimethylformamide, polyacrylonitrile, and $(NH_4)_2CO_3$ was injected into hot-water, a phase separation quickly occurred, which then formed a solid polymer crust. Meanwhile, the CO_2 and NH_3 gas, which decomposed inside the $(NH_4)_2CO_3$, was not able to easily escape. This inner pressure allowed for the formation of a hollow structure. The hollow polyacrylonitrile's mechanical performance could then be enhanced by the introduction of carbon nanotubes (CNTs) as a strengthening agent.

2.2 Structure control

2.2.1 Surface morphology

Carbon surface configuration is of great importance for various applications, and thus having a controllable HCSs preparation with a tunable surface morphology is key. Two methods for this are presented in Fig. 4. Walnut-shaped PDA with a hierarchical meso-macroporous structure were designed through a cooperative assembly of dopamine, dual-soft-template (P123 and F127) and 1,3,5-trimethylbenzene (Fig. 4(a)) [55]. The obtained nanoparticles possessed ultra-large bicontinuous channels of 20–95 nm. By changing the surfactant packing parameter, the mass ratio of P123 to F127 managed to precisely affect the porous structure and morphology of the PDA nanoparticles. By simply elevating the P123/F127 mass ratio, the

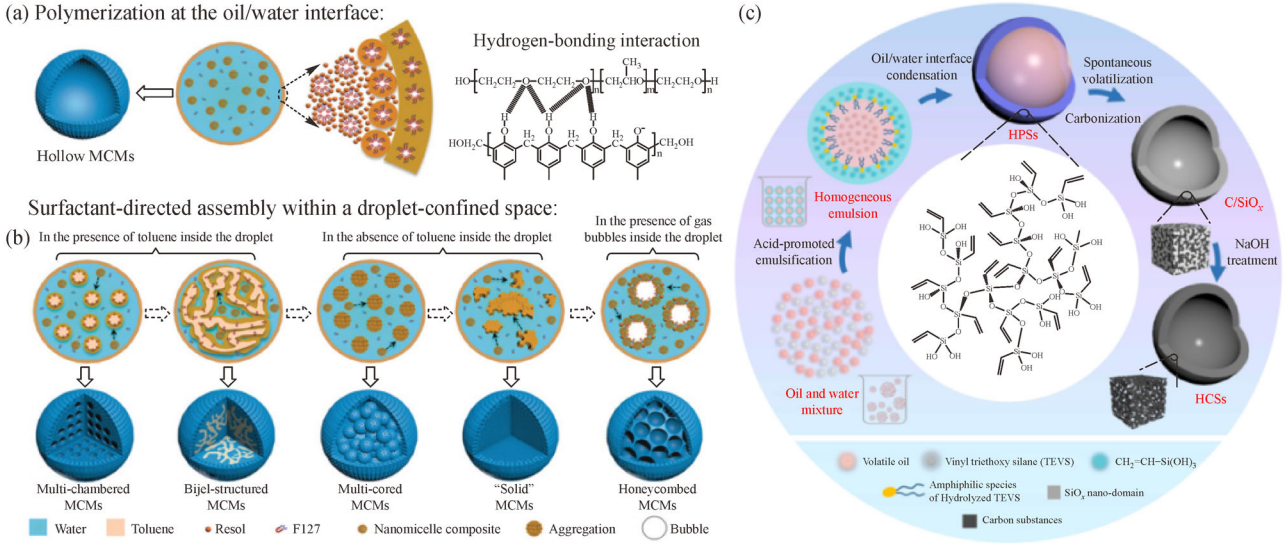

Fig. 2 Formation mechanism of mesoporous carbon microspheres with different interior-structures: (a) Interfacial polymerization of phenolic resol and F127; (b) evolution illustration of the inner structures. Reprinted with permission from ref. [47], copyright 2018 Wiley-VCH. (c) Schematic illustration of HCSs in the presence of organosilane. Reprinted with permission from ref. [48], copyright 2020 Elsevier.

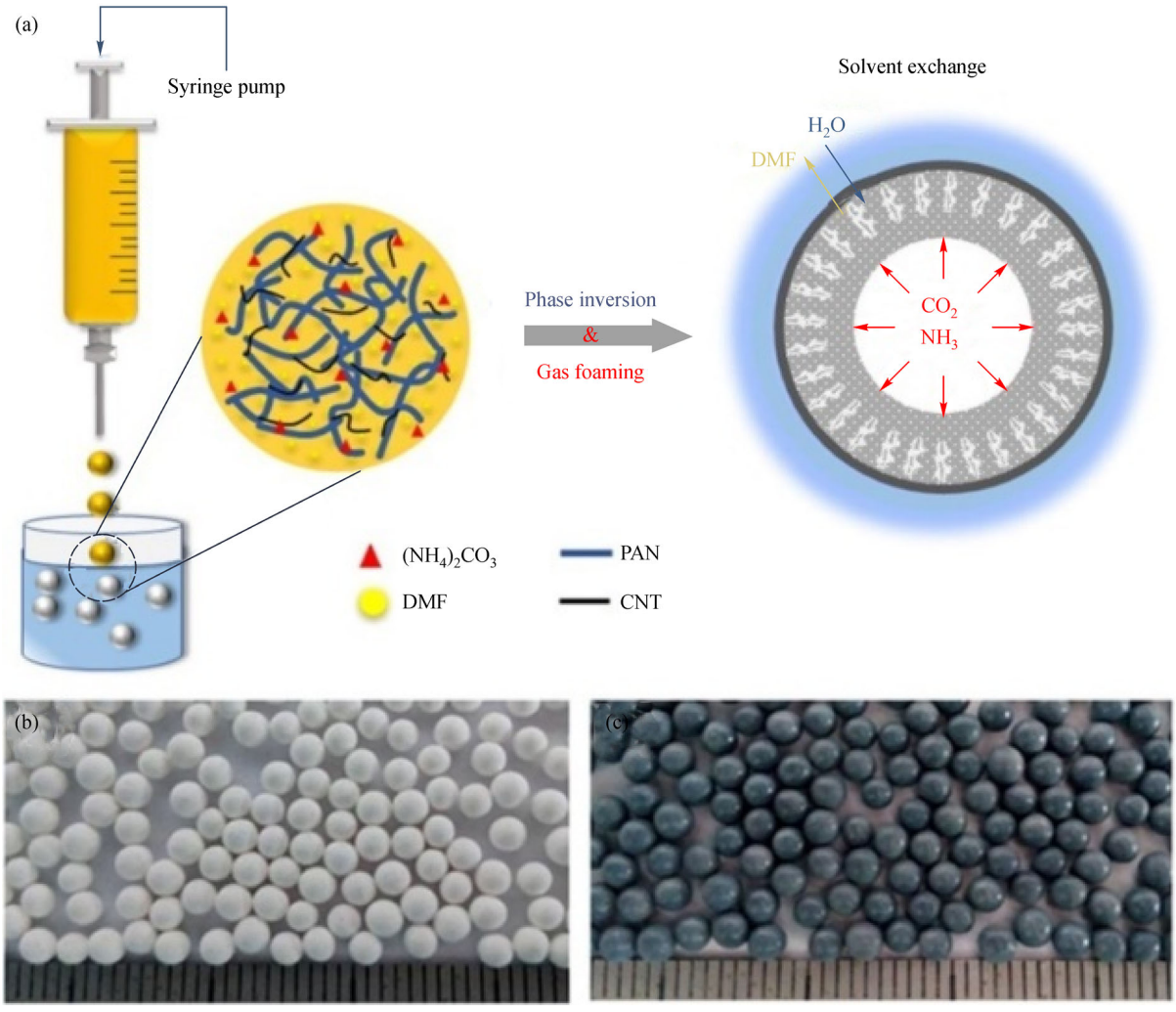

Fig. 3 (a) Schematic illustration for the synthesis of hollow-structured polyacrylonitrile spheres; photograph of (b) hollow polyacrylonitrile spheres, and (c) CNT-enhanced hollow polyacrylonitrile spheres. Reprinted with permission from ref. [54], copyright 2016 Wiley-VCH.

morphology of the PDA products can be transformed from bowl-like to dendritic, and finally to walnut-shaped (Figs. 4(b–k)). Pore architecture was also transformed from columnar to bicontinuous, and finally to a lamellar structure. This highly interconnected porous structure could shorten diffusion resistance and enlarge the effective area, thereby leading the walnut-shaped carbon particles to exhibit an advantageous electrochemical performance.

Our group employed the direct carbonization of MF@resol resin/graphene oxide (GO) composites to design HCSs with a wrinkled surface [34]. The use of GO was indispensable to the formation of this highly wrinkled morphology. The aromatic parts of GO automatically wrinkled to reduce surface tension when the GO sheet bonded to the resol resin through the Coulombic forces between the O-containing groups and resol. Figure 4(m) shows the SEM image of the crumpled surface, which enlarges the accessible surface area and is beneficial to rate capability.

In addition, solvents play an important role in HCSs size and morphology regulation [56]. An example of this is the strong affect that the ethanol/water volume ratio has on HCS morphology [35]. As the ethanol amount increased, the solubility parameter and coating thickness of the mixed solution decreased. The surface of the prepared HCSs changed from smooth to wrinkled and then to con-caved.

2.2.2 Porous structure within the shell

The porous architecture in the HCSs shell is another significant factor to be considered due to this parameter being directly associated with the accessible surface area. Generally speaking, large amount of micropores can be produced through the carbonization of the polymer-based

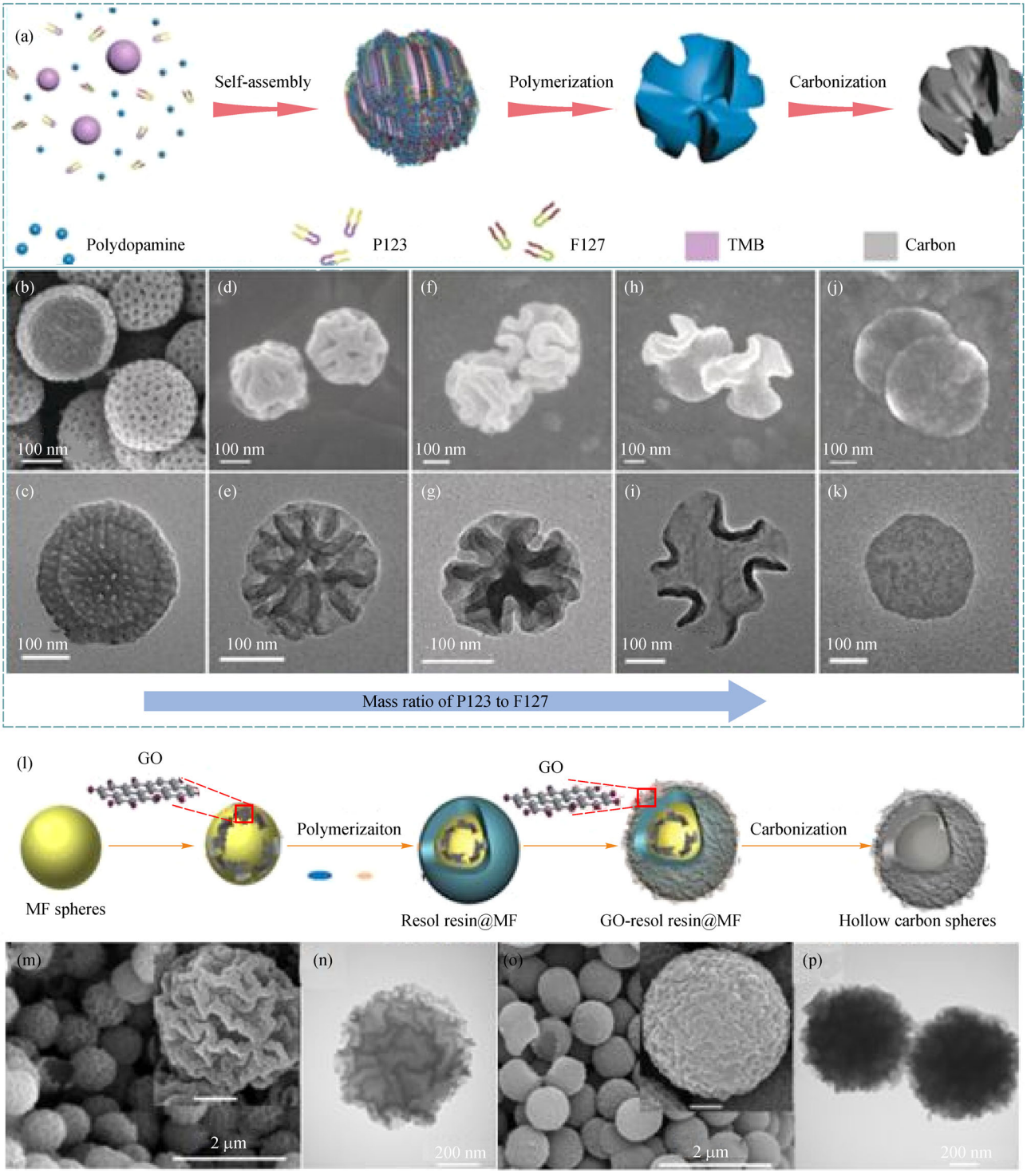

Fig. 4 (a) Schematic illustration for the preparation of walnut-shaped PDA; (b–k) field emission scanning electron microscope (SEM, top) and TEM (bottom) images of PDA prepared by P123 to F123 mass ratio tuning. Reprinted with permission from ref. [55], copyright 2018 Wiley-VC. (l) Schematic illustration for the synthesis of NHCSs. SEM and TEM images of (m, n) NHCSs and (o, p) NHCSs without using GO. Reprinted with permission from ref. [34], copyright 2016 Royal Society of Chemistry.

carbon precursor (such as resol resin, dopamine and so on). Thus, the HCSs fabricated from these precursors usually have a microporous shell.

HCSs with mesoporous shells have been receiving increasing attention due to their interconnected mesoporous channels providing large accessible interior space for faster ion transportation [57]. Mesoporous HCSs with a pore size of 2–20 nm can be prepared with the aid of

various block polymers working as the mesopore-forming agent in the coating process. Resins or other polymers can assembled with surfactants (e.g., cetyltrimethyl ammonium bromide, P123, F127 and other high-molecular-weight block copolymers) through hydrogen-bonding, electrostatic interaction or adsorption [45]. The self-assembly process in the coating layer is similar to the synthesis process of ordered mesoporous carbons. Furthermore, it is well-known that the higher the molecular-weight, the larger the mesopore size. For instance, hollow mesoporous carbon spheres were prepared by assembling polyaniline-co-polypyrrole and Triton X-100, and after carbonization, nanopores with a maximum peak at 2.5 nm were observed in its carbon shell [58]. NHCSs with large mesopores of up to 16 nm could be fabricated by using high-molecular-weight polystyrene-*block*-poly(ethylene oxide) as the template [59]. To achieve larger mesopores, nano-sized SiO_2 particles with a diameter of about 50 nm were used to create a tunable open-framework structure with pore sizes ranging from 18 to 30 nm [60].

In order to enrich the shell's porous structure, a "silica assisted" sol-gel strategy was proposed. Using tetraethyl orthosilicate (TEOS) or tetrapropyl orthosilicate (TPOS) is crucial to the generation of hollow cavity and mesoporous shell in this method. With the assistance of cationic surfactant hexadecyl trimethylammonium chloride, Qiao et al. polymerized RF resin and TEOS, gaining mesopores of 4.7 nm in the carbon shell [61]. It was found that on the basis of the polymerization kinetics, TPOS carried slower hydrolysis and nucleation processes than TEOS, and therefore the silica core and primary particle were better controlled. By changing the ratios of TEOS/TPOS or ethanol/water, the pore diameter of HCSs could be finely manipulated from micropores to 13.9 nm [62].

The microstructures of hollow mesoporous carbon spheres are more precisely regulated by controlling the TPOS hydrolyzation and phenolic resin polymerization process (Fig. 5) [63]. For example, the hollow void is related to the diameter of silica core, which can be enlarged by prolonging the hydrolysis time. The mesopores in the carbon shell were associated with the size of the embedded SiO_2 nanoparticle. The volume ratio of water to ethanol determined the SiO_2 nanoparticle as a result of TPOS hydrolyzed faster in water than in ethanol. Controllable constructions, including hollow voids (89.3–204.5 nm), mesopores (7.1–11.3 nm), and shell thickness (68.1–148.7 nm) could be fabricated.

In addition, activation methods that handle carbons with specific chemicals (KOH, $ZnCl_2$ and H_3BO_3) or gases (steam, and CO_2) are popular for the creation of a large amount of mesopores. For the HCSs from the hard-templating method, the released gases (CO_2, N-containing alkaline gas) from the decomposition of the templates ($CaCO_3$, MF spheres and PMMA spheres) can active the carbon shell and benefit the generation of mesopores, thereby yielding a highly mesoporous structure with a large surface area. Unfortunately, it is usually impossible to control the pore formation.

In electrochemical applications, large macropores can act as a buffering reservoir to minimize the transmission distances of the guest species into the inner surface. As demonstrated in Fig. 6, co-assembly of MF resin and SiO_2 nanospheres was used to configure a hierarchical micro-, meso-, and macroporous structure into the shell of N, P co-doped hierarchical porous carbon microspheres (NPHCMs) (Fig. 6(a)) [64]. The NPHCMs had a particle size of ~14 μm, as well as a number of macropores on the shell (Figs. 6(b–f)). The open macropore windows (250 nm) originated from the etching of the SiO_2 spheres. Additionally, a mesoporous structure with pore sizes of 2.6 and 3.7 nm also appeared in the shell.

2.3 Functionalization of HCSs

2.3.1 Heteroatom doping

Heteroatom doping can strengthen conductivity and improve the hydrophilicity of HCSs, and shows remarkable influence on specific applications. There are two main ways to incorporate heteroatoms into the carbon framework: one is *in-situ* doping, where the heteroatom-containing carbon precursor, catalysts and other assistants is employed to build the carbon skeleton; the other is post-incorporation, where heteroatoms containing gas or liquid are used to activate the carbon framework and further introduce foreign atoms. Of the two methods, *in-situ* doping is the most convenient, and its content of heteroatoms is always higher than from the post-treatment approach.

N is the most popular heteroatom among the doped materials. PDA [29,55], 3-aminophenol [65], glycine [66], and melamine [34,35,44,64] have been served as N-containing carbon sources to fabricate NHCSs. The N content in the NHCSs is directly determined by the raw materials and so in order to incorporate more N into the carbon framework, a substance with a high N concentration is required. As presented by Fig. 7, graphitic carbon nitride (g-C_3N_4) nanosheets, as an N-rich graphite (~57.1 at%), was used as the precursor to tune the N-doping properties of NHCSs. For this process, Zn powder was employed as both the template and catalyst (Fig. 7(a)). A carbonization temperature above 700 °C was required for the formation of roll-like N-doped carbon (NC) on the melting Zn particles surface. The N-doping level was as high as 12.76–27.82 at% and the doping types were easily tuned by controlling the synthetic temperatures [39]. EDA with a high N content of 46.6 wt% also contributed to the N source by participating in the interfacial sol-gel coating and producing a homogeneous N doping of 8.23 wt% [67].

Some other heteroatoms, such as B, S and P, have also proved to be of great interest. Coville's group prepared

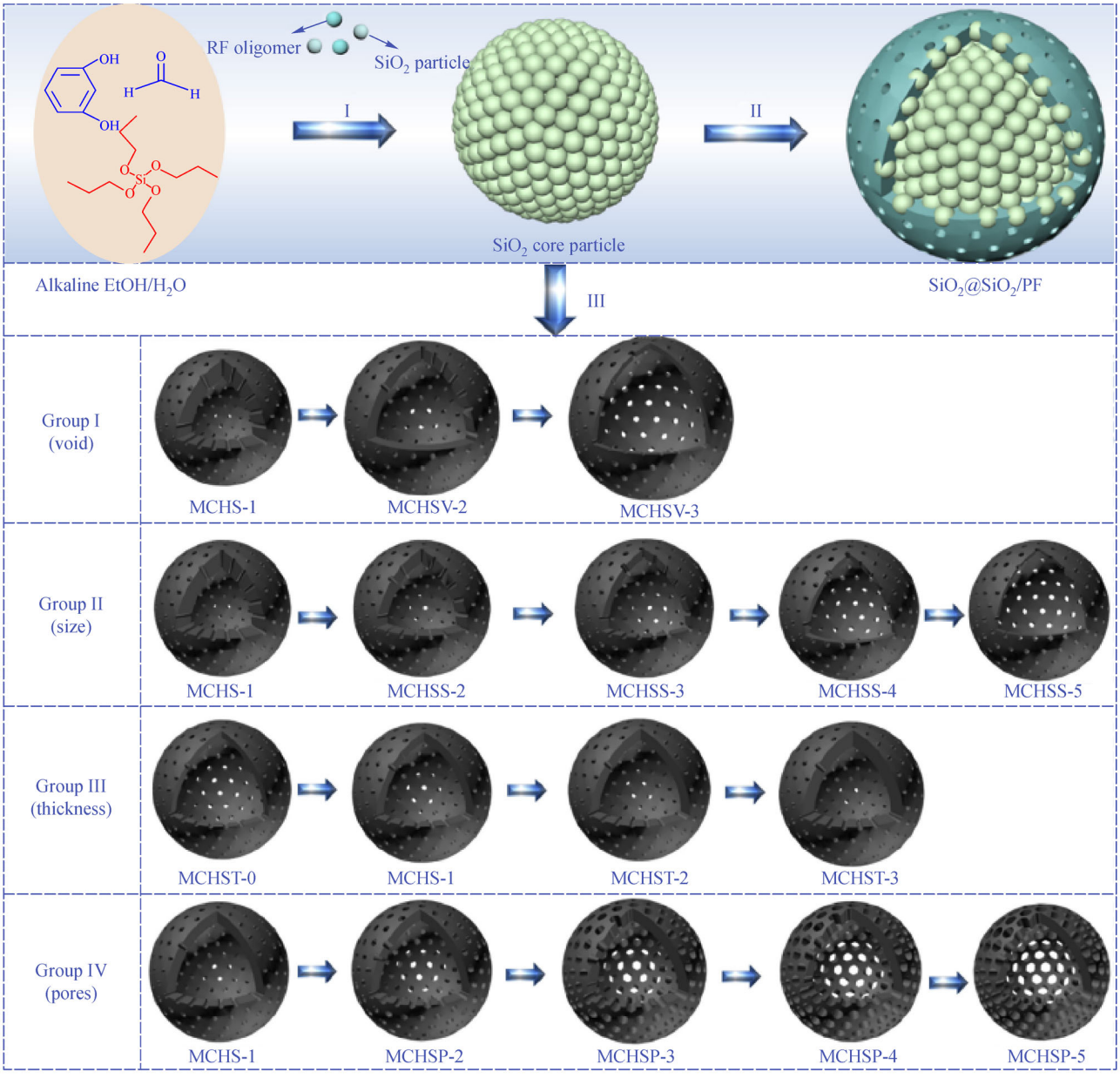

Fig. 5 The synthesized mechanism and controlled structure parameters of mesoporous HCSs, including hollow void size (group I), integrate size (group II), carbon shell thickness (group III) and mesopores in carbon shell (group IV). Reprinted with permission from ref. [63], copyright 2016 Elsevier.

boron-doped HCSs by using trimethyl borate or BCl_3 as the boron source via a high temperature chemical vapor deposition [68,69]. S and P atoms have larger atom radii than N, and their easily polarized lone pair electrons can further boost the chemical properties and more effectively increase defects. P-doped HCSs were prepared using tetraphenylphosphonium bromide as the P source, and glucose as the C source through a soft-templating method [70]. Besides single atom doping, either P or S is always doped into the carbon skeleton along with N. The synergistic effect of these two heteroatom types can enhance the electrochemical performance. Two or more of the N, P, and S heteroatoms are co-doped into a carbon framework and extensively investigated. Ni et al. [71] used PDA as the nitrogen precursor and $CaCO_3$ as the template to synthesize the N-doped mesoporous HCSs. The S and N co-doped HCSs were further realized by treating the N-doped mesoporous HCSs under an Ar/H_2S mixed atmosphere.

In general, the interactions of the dopants with the carbon sources affected the doping uniformity and doping content in the carbons. By using heteroatom-containing catalysts to polymerize MF, N, P co-doped and N, S co-doped hierarchical porous carbon microspheres were

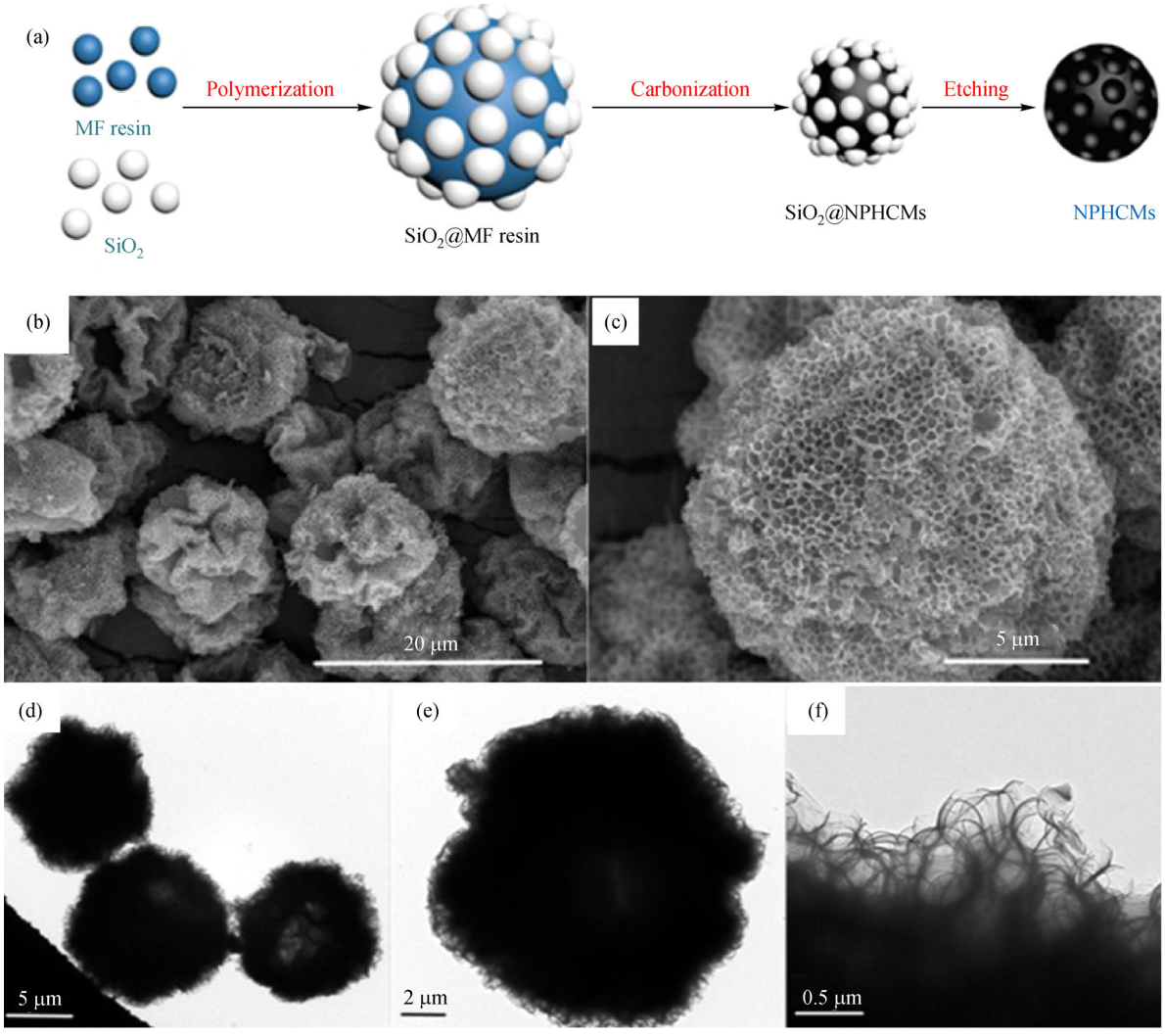

Fig. 6 (a) Illustration of the formation mechanism in NPHCMs; (b, c) SEM and (d, e, f) TEM images of NPHCMs. Reprinted with permission from ref. [64], copyright 2017 Royal Society of Chemistry.

engineered by employing 1-hydroxy ethylidene-1,1-diphosphonic acid (HEDP) as the phosphorus source and methionine as the S source, respectively [64,72]. The weak physical interaction between HEDP and MF resulted in a low P doping of 0.16%. Further research used phytic acid to crosslink polypyrrole, and the fabricated homogeneous crosslinked structure favored N, P co-doped HCSs with a high N and P content of 11.4 and 3.5 wt%, respectively [73]. Wang et al. [74] proposed a novel approach by grafting a P-containing modifier hexachlorocyclotriphosphazene (HCCP) onto the SiO_2@PDA shell. As the HCCP molecule had six P–Cl bonds, it could chemically graft hydroxyl and amino groups onto PDA (Fig. 7(b)). After calcination and SiO_2 template removal, NP-HPCS were obtained. Owing to the promoted chemical interaction between HCCP and PDA, the NP-HPCS processed a high-level N, P doping of 6.05 and 5.19 at% respectively, as well as excellent Na storage performance. The recently reported examples of HCSs being prepared via different methods, including templates, precursors, heteroatom doping and the conditions for carbonization, are all summarized in Table 1.

2.3.2 Metal-free HCSs hybrids

Controlling HCS distribution within the reduced GO (rGO) network is a vital step to obtain a homogeneous three-dimensional (3D) interconnected architecture. As represent in Fig. 8, Li et al. [78] and Zhang et al. [22] both developed the same technology. They bridged thin rGO nanoflakes and poly(vinyl alcohol)-assisted spherical MF resin to a homogeneous 3D architecture (Fig. 8(a)) [22]. With the help of poly(vinyl alcohol) acting as both the nucleating agent and dispersant, accompanied by a careful freezing treatment, the monodispersed MF spheres with a uniform diameter of 450 nm were heterogeneously dispersed within the rGO network (Figs. 8(b–e)). HCSs were also used as additives to achieve a high specific surface aerogel. Dong

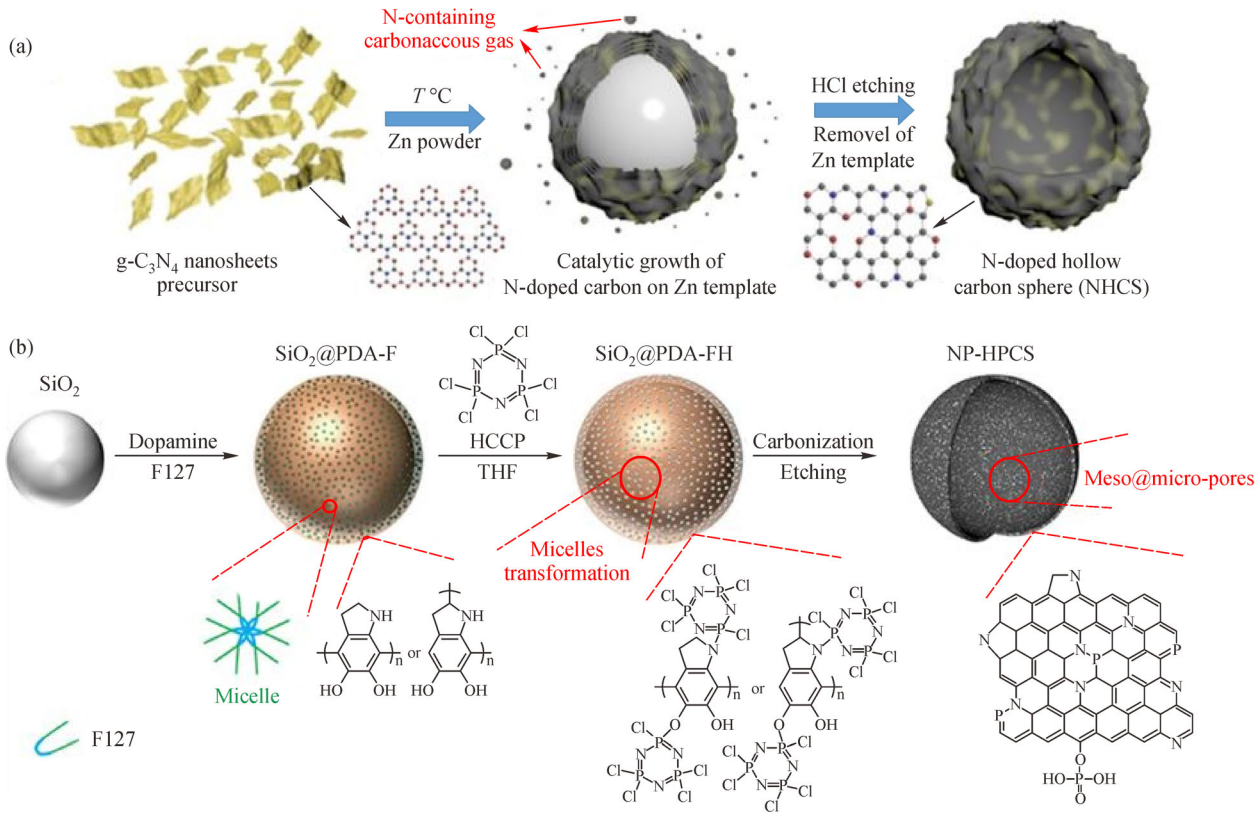

Fig. 7 Graphical illustration of the formation process for (a) NHCSs using g-C_3N_4 as the carbon precursor, and (b) for N, P co-doped hollow porous carbon spheres (NP-HPCS). Reprinted with permission from ref. [39], copyright 2020 Elsevier.

et al. [79] assembled submicron-sized microporous HCSs into graphene aerogels, then fabricating heterogeneously structured bead-to-sheet aerogels. GO was employed as both the dispersion agent to stabilize the submicron spheres, and as a nano-crosslinking agent to crosslink the conjugated polymer spheres through a strong π-π interaction. The HCSs originating from conjugated polymeric hollow spheres were ultra-lightweight with a microporous shell. After a supercritical CO_2 extraction and carbonization, polylithic aerogels were achieved with a low density of 51–67 mg·cm^{-3} and a large surface area of 569–609 m^2·g^{-1}. The cylindrical rod-like polylithic aerogel could unbendingly stand upon the stamens (Fig. 8(f)). SEM and TEM images confirmed that the HCSs had a particle size of 110 nm and that they were wrapped in several graphene layers (Figs. 8(g) and 8(h)).

CNT is another nanocarbon type with excellent conductivity and large pore channels, but it is limited by its relatively low specific surface area. HCSs were anchored onto the surface of CNTs in order to obtain hybrid materials with an enhanced surface area [80]. Subsequently, heteroatom-doping HCSs were encapsulated into one CNT that templated from anodic aluminum oxide, and a spheres-in-tube nanostructure with hierarchical porosity was engineered. The synergistical hybrid structure facilitated the transportation of ions and electrons [81].

2.3.3 Metal-containing HCSs Hybrids

When applied to energy storage and catalysis functions, metal and metal oxide are incorporated into hollow carbons through impregnation, precipitation, or chemical vapor deposition methods. The appealing architecture of HCSs can serve as heterogeneous nucleation centers to anchor metal and metal oxide/sulfide nanoparticles, while simultaneously restraining nanoparticle aggregation.

Noble metal nanoparticles are widely applied in the area of catalysis, and combining them with HCSs can reduce the amount of noble metal, as well as maximize its active surface area. Moreover, the HCSs' large specific surface area and hollow core enable a high dispersal of the nanoparticles and will impede aggregation even at high temperatures, thus enhancing catalytic stability. Noble metal nanocrystals, such as Ru, Ir, Ag, Pd, and PdAg can be encapsulated in the inner voids, or embedded into the HCS shell through a SiO_2 templated two-step coating approach [82–86].

Metal-organic frameworks (MOFs), which contain metal species and organic components, are considered

Table 1 Related information on carbon spheres prepared via different methods

Sample	Template	Precursor	Heteroatom doping	Gas/temperature	Ref.
N-doped yolk-shell HCSs	SiO_2	PDA	N, S	N_2/800 °C	[21]
HCSs	Poly(vinyl alcohol)	Melamine resin spheres	N, O	Ar/700 °C	[22]
NHCSs	Polystyrene spheres	ZIF-67/NIL-101	N	N_2/700 °C	[23]
NHCSs	Polystyrene spheres	Polyaniline	N	N_2/800 °C	[24]
NHCSs	Polystyrene spheres	Polypyrrole-polyaniline	N	N_2/500 °C	[25]
HCSs	SiO_2	Phenolic resin	–	–	[26]
HCSs	SiO_2 spheres	RF	–	N_2/800 °C	[27]
NHCSs	SiO_2 spheres	RF and PVP	N	N_2/600 °C	[28]
DHCS	SiO_2 spheres	PDA	N	Ar/800 °C	[29]
NHCSs	Sulfonated polystyrene spheres	Polyaniline	N	N_2/600 °C	[30]
HCSs	Polystyrene spheres	Glucose	–	N_2/800 °C	[31]
Hierarchical porous HCSs	PMMA	RF	–	N_2/800 °C	[32]
NHCSs	Polystyrene spheres	ZIF-8	N	N_2/800 °C	[33]
NHCSs	MF spheres	Resorcinol and hexamethylenetetramine	N	N_2/800 °C	[34,35]
NHCSs	$CaCO_3$	PDA	N	N_2/800 °C	[36,37]
NHCSs	Yeast cells	Yeast cells	N	N_2/850 °C	[38]
NHCSs	Zn powder	g-C_3N_4	N	Ar/800 °C	[39]
NHCSs	Cu_2O solid spheres	3-aminophenol and formaldehyde	N	N_2/1000 °C	[40]
Hollow carbon nanoparticles	F127	α-cyclodextrin	–	Ar/900 °C	[42]
N-doped mesoporous HCSs	Pentane-1,5-bis(dimethylcetyl ammonium bromide)	3-aminophenol-formaldehyde resin	N	N_2/850 °C	[43]
NHCSs	–	Poly(amic acid) and melamine	N	N_2/800 °C	[44]
Hollow mesoporous carbon microparticles	SiO_2	Poly(furfuryl alcohol)	–	N_2/850 °C	[45]
HCSs	P123 and sodium oleate	Glucose	–	N_2/900 °C	[46]
Mesoporous carbon microspheres	SiO_2	Phenolic resol	–	N_2/600 °C	[47]
HCSs	Volatile oils	Organosilane	–	N_2/900 °C	[48]
HCSs	SiO_2 spheres	Polystyrene and divinylbenzene	N	N_2/700 °C	[49]
Sub-micron HCSs	–	Soybean waste	–	N_2, H_2O/850 °C	[50]
N-doped hollow carbon nanospheres	–	ZIF-8	N	Ar/800 °C	[51]
N, S doped HCSs	–	Puffball spores	N, S	N_2/800 °C	[52]
HCSs	Gas bubbles	Polyacrylonitrile	–	N_2/900 °C	[54]
NHCSs with macro-/mesoporous channels	P123, F127, 1,3,5-trimethylbenzene	PDA	N	N_2/800 °C	[55]
NHCS with large mesoporous shells	Polystyrene-*block*-poly(ethylene oxide)	PDA	N	N_2/800 °C	[59]
NPHCMs	SiO_2 spheres	MF resin and HEDP	N, P	N_2/800 °C	[64]
N-doped mesoporus HCSs	$CaCO_3$ spheres	PDA	N, S	Ar and H_2S/800 °C	[71]
NP-HPCS	SiO_2 spheres	PDA and HCCP	N, P	N_2/900 °C	[74]

emerging candidates for the production of metal (oxide)/hollow-structured carbons through direct pyrolysis [87,88]. Zhang et al. [23] prepared Co-Fe alloy/NHCSs through pyrolysis of dual-MOF (MIL-101/ZIF-67) architecture. As shown in Fig. 9, the MIL-101/ZIF-67 composite was first coated on the polystyrene spheres template. During the annealing process, the core of the polystyrene transformed into a hollow void, the organic

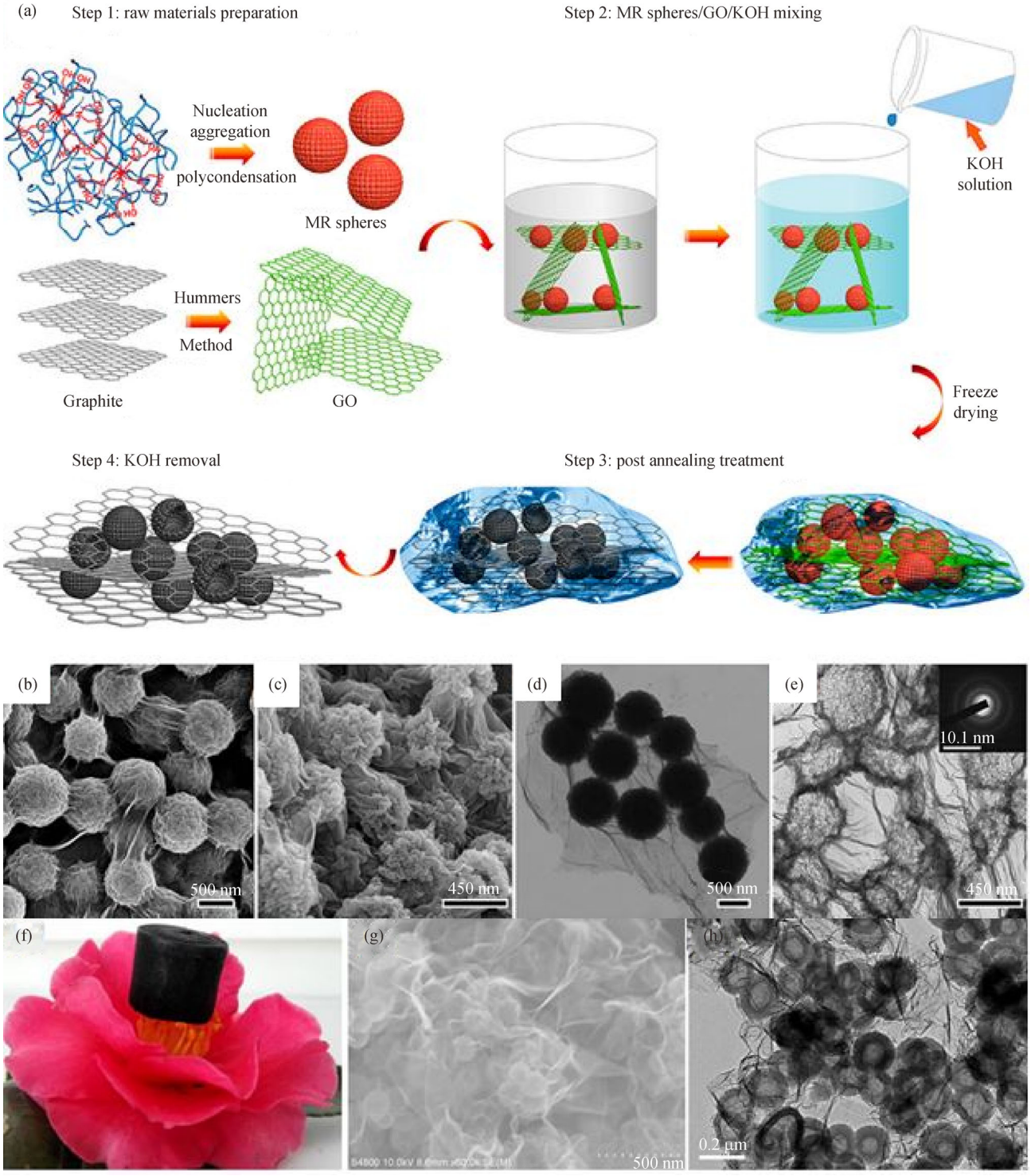

Fig. 8 (a) Schematic illustration for the preparation of HCSs/RGO composites. SEM and TEM images of (b, d) MF spheres/GO and (c) HCSs/RGO-700. Reprinted with permission from ref. [22], copyright 2018 American Chemical Society. (f) Photo of resulting aerogel monolith on a flower bud; (g) SEM image; (h) TEM image of polylithic aerogels. Reprinted with permission from ref. [79], copyright 2016 Elsevier.

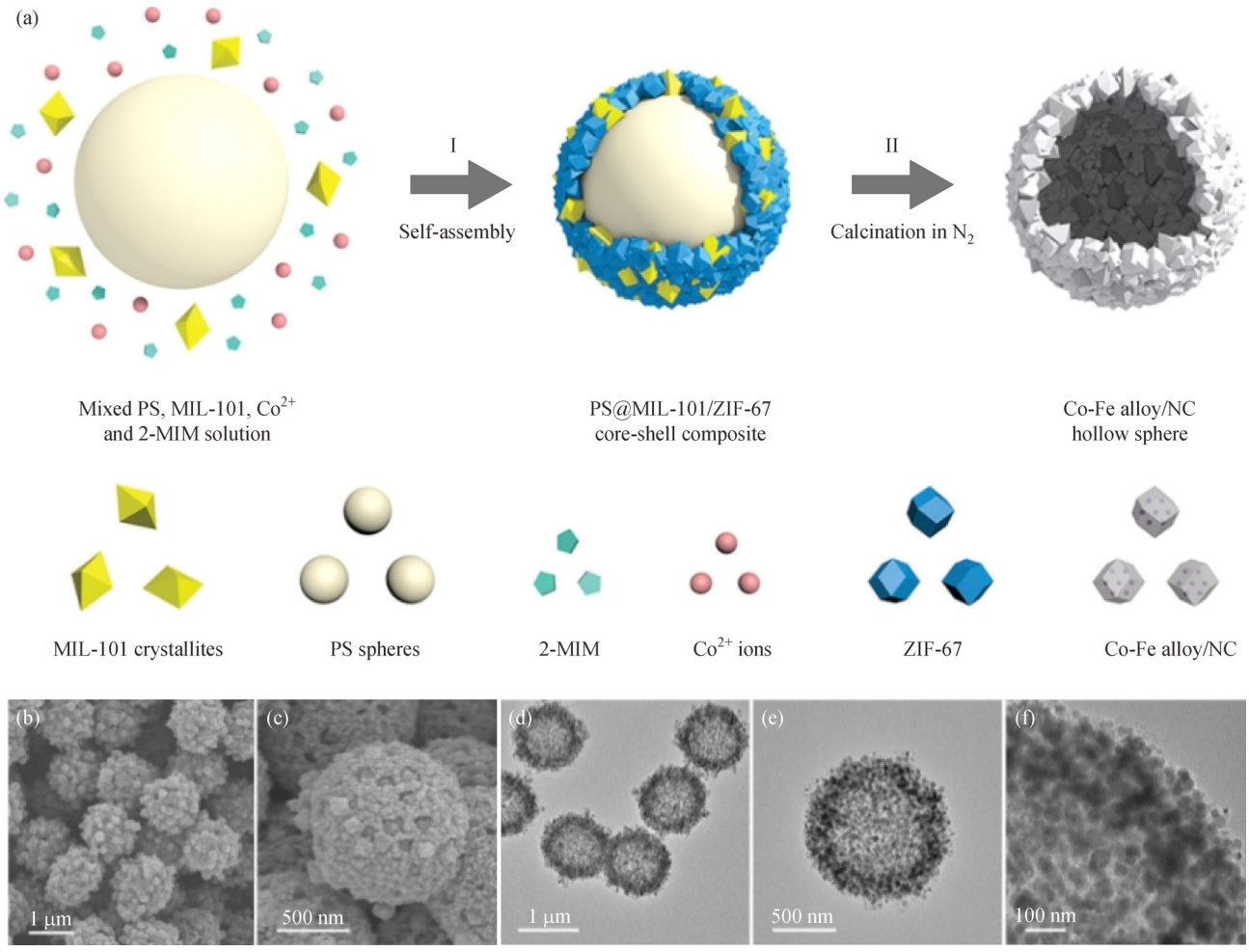

Fig. 9 (a) Schematic illustration of the fabrication process for Co-Fe alloy/NHCSs; (b, c) SEM images; (d, e, f) TEM images of Co-Fe/NC-700 HCSs. Reprinted with permission from ref. [23], copyright 2019 Wiley-VCH.

ligands in the MOF were converted into an NC skeleton, and the Fe^{3+} and Co^{2+} in the shell turned into Co-Ni alloy nanoparticles. Similarly, when using ZnFe-ZIF MOF as the shell and PS as the core, Fe, N co-doped HCSs were fabricated [87].

Impregnation of a metal source into the pores of the carbon shell, followed by carbonization is the most used approach for the production of metal oxides/sulfide hybrids, such as Co_2NiO_x [89], Co_3O_4 nanosheets [90], and Fe_3O_4 [91]. For instance, Hao et al. [92] reported on the creation of FeO_x@N, P-doped HCSs by coating PDA/Fe^{3+} shell onto the MF spheres. Wang's group [93] utilized a similar melting-diffusion strategy to group the Fe_3O_4 nanoparticles into the inner wall of the NHCSs.

3 Noble metal-free catalysis

Noble-metal (Pt, Ru)-based catalysts are highly efficient for many reactions, but are limited by their scarcity and high cost. In recent years, the development of effective and stable metal-free and non-precious metal catalysts has become a hot topic in scientific fields. The HCSs' a-typical voids and high surface area provide more available space to expose the abundant active sites. Furthermore, by designing the electronic and structural properties, the HCSs' electrochemical performances can be further enhanced, thereby making them advantageous for applications in energy conversion, storage and pollutant degradation.

3.1 Oxygen reduction reaction (ORR)

ORR constitutes a major cathode-reaction for metal-air batteries and fuel cells, and occurs through a two-electron or four-electron pathway. The two-electron pathway can reduce oxygen to H_2O_2, while a four-electron process usually achieves water. Both processes are related to the interaction between the reactive intermediate *OOH and the catalysts. The strong binding of *OOH favors H_2O production while the weak interaction facilitates the formation of H_2O_2. Metal-free carbon materials

[25,55,70,94,95], transition-metal phosphate [96], and transition metal nitrides/oxides/carbides/sulfides [5,89,97] have all been intensively developed as catalysts for ORR.

3.1.1 Two-electron ORR

A two-electron pathway ORR is an on-site method that can be operated at room temperature in a wide pH range to directly generate H_2O_2. This two-electron process requires fast oxygen adsorption and *OOH intermediate desorption. For carbon-based catalysts to produce H_2O_2, many important factors, including pore size, heteroatom-containing functional groups (e.g., O, N, S and F), defect sites and surface charges, are required to affect the overall catalytic performance [98,99]. Mesoporous carbon hollow spheres obtained from a SiO_2-templated sol-gel process were used as metal-free ORR catalysts to effectively produce H_2O_2. In comparison to micropores, the mesoporous structure played an important role by enhancing mass transfer to lower onset potential and boost catalytic activity. The surface O-containing groups, especially the COOH groups, were beneficial for the production of H_2O_2, which elevated H_2O_2 selectivity. This catalyst exhibited an H_2O_2 selectivity of over 90% in a potential range of 0.35–0.62 V under neutral conditions (0.1 $mol \cdot L^{-1}$ phosphate buffered saline) and reached its maximum (99.9%) at 0.57 V [94]. Moreover, these foreign dopants can introduce more activated π electrons and thus further increase the active center density [100,101]. Inspired by the fact that the S dopant can motivate carbon to adsorb O_2 and further reduce overpotential, single S crystals were confined into the pores of the HCSs that had been obtained from the SiO_2-templated approach [102]. As a result of the channel confinement effect, the formed S nanocrystals were in a nanoscale of 2–5 nm. Compared with the S-free samples, the composite had a boosted H_2O_2 selectivity of 70% and a low overpotential of 0.01 V (in 0.1 $mol \cdot L^{-1}$ KCl). Through density functional theory (DFT) calculations, it was confirmed that the C–S edge sites were the active sites, and that the S–S bond markedly enhanced selectivity.

Introducing two heteroatom types into the carbon skeleton can further improve the catalytic production of H_2O_2 due to the synergetic effect between the doped foreign atoms. The synergetic effect has been observed in N and F co-doped carbon nanocages fabricated by DA polymerization (N source) on polyvinylidene fluoride spheres (fluoride source) [103]. The doped N atoms proved beneficial to O_2 adsorption, which thus facilitated the catalytic activity, while F doping favored the release of *OOH, thereby creating high H_2O_2 selectivity. The N and F co-doped carbon nanocages efficiently catalyzed H_2O_2 electroproduction with a high faradaic efficiency of 89.6% in alkaline solution (pH = 13, 0.74 V), and 85%–88% in acid electrolyte (pH = 0.35, 0.4–0.72 V).

Light-driven catalytic production of H_2O_2 through two-electron reduction is another type of green chemistry process. Benefiting from its large accessible surface area for charge transfer and photo-absorption, hollow-structured P-doped g-C_3N_4 can effectively produce H_2O_2 through two-electron O_2 reduction. The doped P was regarded as an indispensable attribute that significantly improved the catalytic performance by tuning the energy band, promoting carrier mobility and enhancing H_2O_2 selectivity. The P-doped g-C_3N_4 hollow spheres had an improved H_2O_2 production rate (174 $\mu mol \cdot h^{-1}$ in H_2O, 1684 $\mu mol \cdot h^{-1} \cdot g^{-1}$ in isopropanol), with values almost 7.5 and 11.2 times higher than bulk g-C_3N_4 [104]. In addition, the doped carbons can coordinate with non-nobel metal and so endow them with high catalytic activity. In this way, Cu-doped g-C_3N_4 produced 10.7 fold more H_2O_2 than neat g-C_3N_4 [105]. The coordinative Cu(I)-N active sites acted as both adsorption sites to motivate the O_2 molecules, and as an "electron transfer bridge" that accelerated the electron transfer from Cu-doped g-C_3N_4 to the adsorbed O_2.

3.1.2 Four-electron ORR

The four-electron ORR pathway is considered energetically favorable in thermodynamics, meaning that it occurs easily compared with the two-electron process. Highly effective $4e^-$ ORR electrocatalysts can be obtained through an engineering of their electronic structure. One of the most famous strategies to modulate electronic structure is heteroatom-doping. It has been demonstrated that the NC electrocatalysts, especially the pyridinic-/graphitic-N, play an important role in promoting the four-electron process [25,70,100]. Pyridinic-N offers a more positive onset potential by moving down the energy barrier of O_2 adsorption, and also facilitates the ORR kinetic. Graphitic-N is favorable in limiting current density by improving electrical conductivity and providing more valence electrons. Pyridinic- and graphitic-N enriched hollow mesoporous carbon nanospheres showed an onset potential of 0.84 V and a lower Tafel slope of 65 $mV \cdot dec^{-1}$ in 0.1 $mol \cdot L^{-1}$ KOH [106].

Multi-heteroatom-doping can give rise to a favorable electron-donor property, and the synergistic effect is preferred in order to achieve a high electrocatalytic performance. N, S co-doped HCSs with mesoporous shells were synthesized by polymerization of PDA and sodium 1,5-naphthalenedisulfonate on mesoporous spherical SiO_2 [95]. Owing to synergistic N and S co-doping, and the fast reactant diffusion by hierarchical porous structure, a considerable activity (onset potential = 0.945 V, limiting current density = 5.36 $mA \cdot cm^{-2}$), long-term stability (92% after operation of 20000 s), and a remarkable methanol resistance were obtained in the alkaline solution. Additionally, O, N co-doping was shown to be an effective strategy for the $4e^-$ ORR process. 3D structured O and N co-doped graphene hollow spheres (O,N-graphene) were fabricated by carbonizing Zn-based MOF and subsequent

high-temperature treatment in an NH_3 atmosphere [107]. The large specific surface area (1801.4 $m^2 \cdot g^{-1}$), highly conductive graphene framework, and pyridinic N defects were favorable to accelerate O_2 diffusion and increase the number of active sites. The O,N-graphene presented an onset potential of 1.01 V, a half-wave potential ($E_{1/2}$) of 0.842 V (*vs*. RHE, reversible hydrogen electrode), and high stability (95.8% retention after 10 h) in 0.1 $mol \cdot L^{-1}$ KOH.

Hybridizing the metal-contained component with HCSs is advantageous for the optimization of four-electron ORR activity. The synergistic effect of the metal species and carbon materials can effectively optimize the intermediate adsorption capacity, and lead to a much higher ORR activity. For example, the transition metal modified NCs, especially transition metal-nitrogen-carbon (M-N-C), are considered to have great potentials for replacing Pt-based catalysts through a four-electron pathway [108]. The coexistence of Fe/Fe_3C and Fe-N_x in N-doped carbonaceous frameworks has been identified as a highly effective ORR catalyst in alkaline or acidic conditions over a wide pH range [109]. As Fig. 10 depicts, Tan et al. fabricated Fe-N-doped HCSs with a diameter of less than 50 nm, after which Fe_3C nanoparticles were encapsulated into the shell of HCSs [110]. In this process, poly(styrene-*b*-2-vinylpyridine-*b*-ethylene oxide) was used as the surfactant to enable the formation of a hollow core, while MF resin introduced N (Fig. 10(a)). The Fe_3C-Fe,N/C-900 had a hollow core of 16 nm and a thin shell of ~10 nm (Fig. 10 (b)). Ultra-small Fe_3N nanoparticles were dispersed in the shell (less than 4 nm), which was surrounded by graphitic layers (Figs. 10(b–d)). This catalyst showed satisfactory catalytic activity in terms of $E_{1/2}$ = 0.881 V in 0.1 $mol \cdot L^{-1}$ KOH and 0.714 V in 0.1 $mol \cdot L^{-1}$ $HClO_4$. In the acidic medium in particular, Fe_3C-Fe,N/C-900 showed a limited current density of 5.35 $mA \cdot cm^{-2}$ at 0.3 V.

3.2 Hydrogen evolution reaction (HER)

Hydrogen is regarded as one of the cleanest energies and as a consequence, has attracted increased attention over the past decade. HER is an essential half-reaction of electrochemical water splitting. The most efficient HER catalyst is considered to be the Pt-based catalyst, but unfortunately due to its high cost, it is limited. Currently, transition-metal (Fe, Co, Ni, and Mo)-based electrocatalysts, such as the phosphides/carbides/sulfides [111–114], and metal-free carbons [100,115] are being reported as excellent candidates over HER. Theoretical investigations have found that HER activity is directly related to the H_2 adsorption free energy, and therefore, a balance between the protons transfer and the adsorbed H_2 desorption is needed to achieve high HER activity. When introducing heteroatoms to engineer the electron structure [115], the N-, O- and P-doped HCSs, which had been fabricated by the pyrolysis of Co_2P-containing polypyrrole, exhibited a high electrocatalytic HER activity. A low overpotential (290 mV at 10 $mA \cdot cm^{-2}$), low Tafel slope (102 $mV \cdot dec^{-1}$), as well as high stability were achieved. The multi-heteroatom-doping induced a synergistic effect and the abundant active sites were indispensable to the outstanding electrocatalytic performance.

Transition-metal phosphides are receiving considerable attention as a widely studied and highly efficient catalyst. As described in Fig. 11, encapsulating transition-metal phosphides into NHCSs can elevate catalytic stability and inhibit nanoparticles agglomeration. In this study, MoP nanoparticles were incorporated into the shell of the spherical structured NC (denoted as MoP@NCHSs) through the oxidation of pyrrole monomers by $H_3PMo_{12}O_{40} \cdot nH_2O$ on the polystyrene spheres (Figs. 11(a–c)) [116]. The 900 °C-carbonized sample (MoP@NCHSs-900) exhibited remarkable activity and stability, affording an overpotential as low as 92 mV at 10 $mA \cdot cm^{-2}$ with a Tafel slope of 62 $mV \cdot dec^{-1}$ (Figs. 11(f) and 11(g)) in alkaline media. In-depth insights indicated that pyridinic-N was the predominantly contributing factor to the excellent catalytic activity. The interaction between MoP and pyridinic-N led to elevated electron density on the N-atoms and reduced the *d* band center of Mo. The weakened Mo–H bond reduced the H_2 adsorption free energy and thereby favored H_2 evolution. Hybrid molybdenum disulfide/selenide (MoS_2, $MoSe_2$, $CoSe_2$-$MoSe_2$) has also been demonstrated to perform robust activities for electrocatalytic HER [117,118]. Core-shell structured NHCSs/P-doped MoS_2 (N-C@P-MoS_2) possesses advantageous features, such as having a modified electronic structure, enhanced conductivity, and abundant active sites derived from N and P doping, which are favorable in HER activities [119]. In comparison to single-metal transition-metal phosphides, double-metal phosphides possess a higher electron transfer efficiency. Hollow-structured hybrids composed of NiCoP and N, P-doped carbon exhibit a low overpotential for HER in a wide pH range (108, 128 and 106 mV at 10 $mA \cdot cm^{-2}$ in acidic, alkaline and neutral solution, respectively) [120].

Recently, photocatalytic water splitting has also been described as an environmentally friendly method for H_2 production. Compared with commonly used semiconductor materials, two-dimensional nanostructures (transition metal dichalcogenide, MXene, g-C_3N_4) are considered emerging photocatalysts benefiting from their favorable electronic structures and large surface area for active site exposure [121]. For example, Li et al. prepared g-C_3N_4 hollow spheres (CCNHS) by treating a cyanuric acid-melamine complex using molten salt. The highly crystalline CCNHS had a high surface area of 185.6 $m^2 \cdot g^{-1}$ and a nanorod morphology with a lattice distance of 0.33 nm. These features offered an enhanced migration from the charge carriers, and an increased number of accessible active surface sites. The CCNHS realized a photocatalytic hydrogen generation of 151.2 $\mu mol \cdot h^{-1} \cdot g^{-1}$ [122]. In order

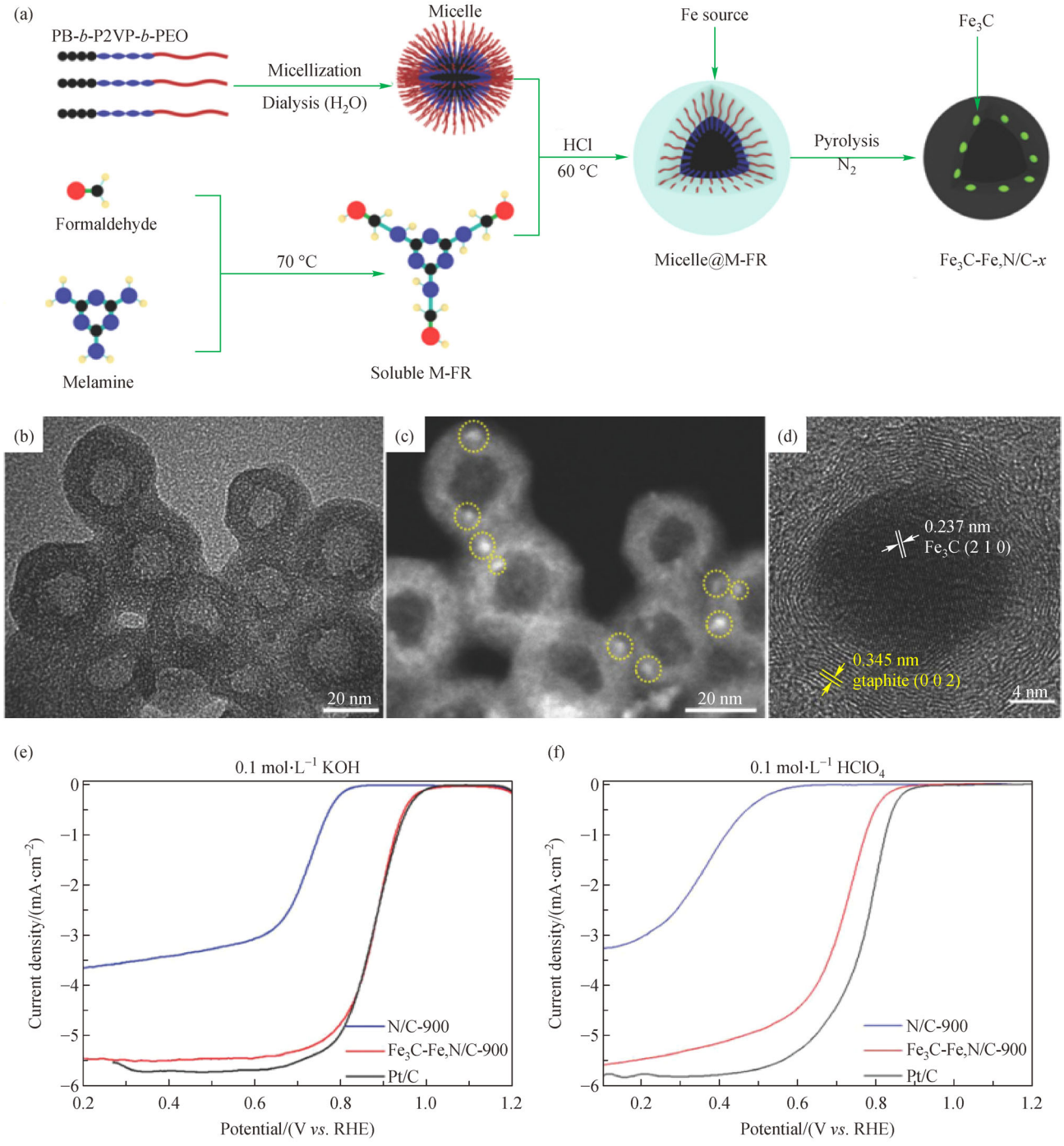

Fig. 10 (a) Illustration of the synthesis process and (b, c) electron microscope images of Fe_3C-Fe,N/C-900 hollow spheres; (d) HRTEM image of a typical Fe_3C nanoparticle; (e, f) linear sweep voltammetry curves of N/C-900, Fe_3C-Fe,N/C-900, and Pt/C at 1600 r·min^{-1}. Reprinted with permission from ref. [110], copyright 2018 Wiley-VCH.

to further elevate light absorption and reduce the charge carrier recombination in g-C_3N_4, the g-C_3N_4/$Ti_3C_2T_x$ hollow architecture was designed. This was achieved by assembling $Ti_3C_2T_x$ and g-C_3N_4 onto polystyrene spheres through an electrostatic interaction-induced layer-by-layer approach. The g-C_3N_4/$Ti_3C_2T_x$ hollow hybrids exhibited an improved light absorption efficiency and charge separation. A much higher H_2 production rate of 982.8 μmol·g^{-1}·h^{-1} was achieved [123].

3.3 Oxygen evolution reaction (OER)

OER is a critical element in the water splitting process, metal-air batteries and CO_2RR flow cells, which always

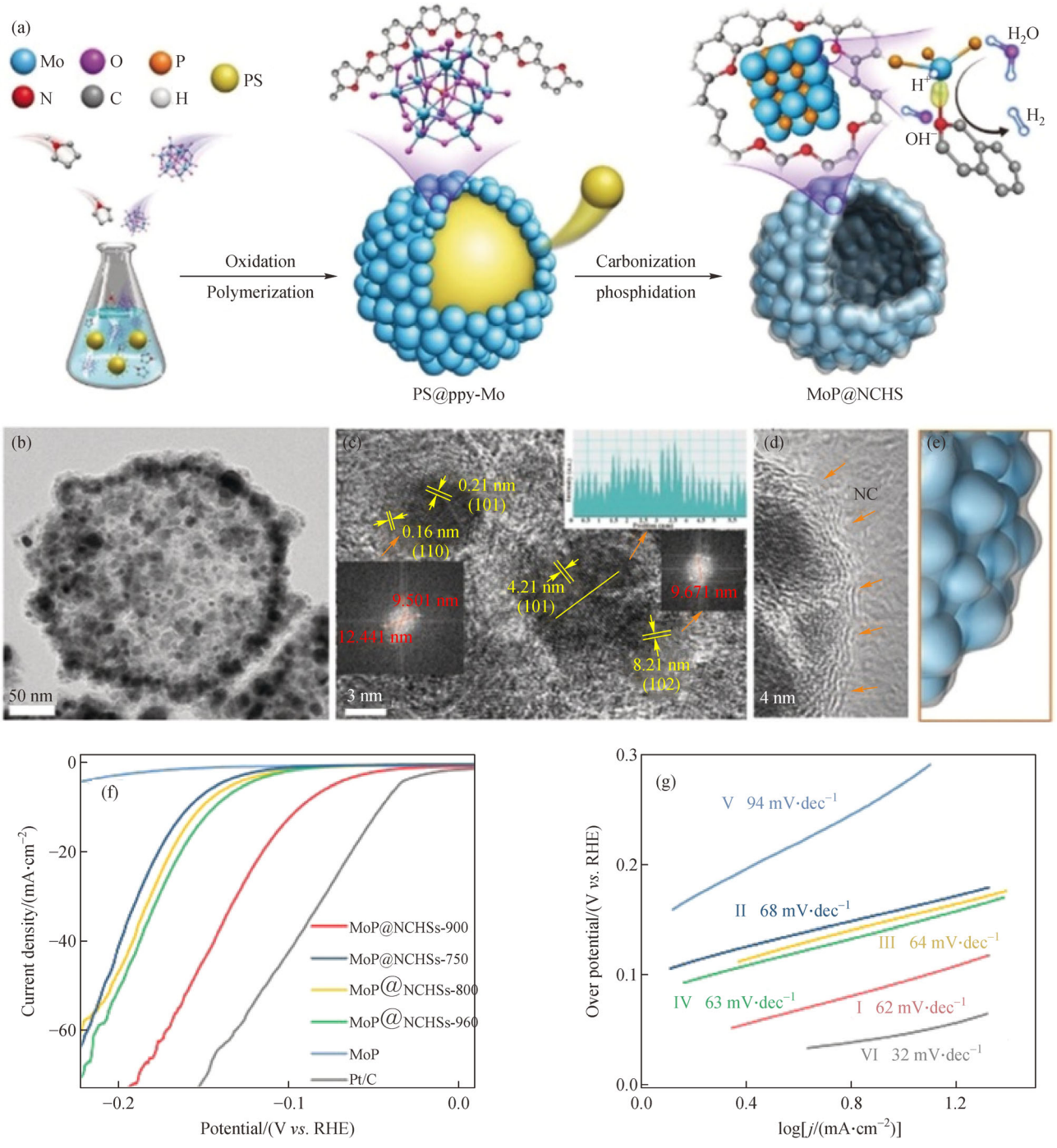

Fig. 11 (a) Schematic presentation of MoP@NCHSs-900 synthesis; (b, c, d) TEM and HRTEM images of MoP@NCHSs-900; (e) structural model of (d); (f) LSV curves; (g) Tafel plots of different electrocatalysts in 1.0 mol·L^{-1} KOH (I: MoP@NCHSs-900; II: MoP@NCHSs-750; III: MoP@NCHSs-800; IV: MoP@NCHSs-960; V: MoP; VI: Pt/C). Reprinted with permission from ref. [116], copyright 2019 Royal Society of Chemistry.

suffers from intrinsically sluggish kinetics and requires high overpotential. Earth-abundant transition metal-based electrocatalysts (e.g., Fe, Co, and Ni,), and especially their hybrids with heteroatom-doped carbonaceous materials (graphene, CNTs, amorphous carbon, etc.), are powerful candidates with comparable OER activity and stability to noble metal oxides (RuO_2 and IrO_2) [124]. Hybrids composed of hollow cobalt phosphate and N, P co-doped carbons have been shown to be effective OER catalysts, and they exhibited high activity in alkaline solution [125]. In most cases, carbon materials are used as support to prohibit active component aggregation, as well as to

synergistically catalyze the OER reaction. In addition, carbon layers can prevent transition metal corrosion and further promote catalytic stability.

Amorphous metallic/bimetallic oxide possessing abundant active catalytic sites have been considered to be active OER catalysts. As Fig. 12 reveals, N, P co-doped mesoporous carbon hollow sphere (meso-NPC)/Co_2NiO_x hybrids were replicated from mesoporous SiO_2 and worked as an effective OER electrocatalyst (Fig. 12(a)) [89]. The N, P doping brought abundant hydroxyl groups onto the meso-NPC surface, thereby leading to a uniform anchoring of the ultrasmall Co_2NiO_x particles (1.78 nm) through strong interfacial interaction (Figs. 12(c) and 12(d)). X-ray photoelectron spectroscopy proved that the promoted electron transfer from metal (Co_2NiO_x) to carbon (meso-NPC) gave rise to an increased oxidation state of transition metals. In addition, the metal-to-carbon charge transfer could be further boosted by increasing the P dopant in meso-NPC. In comparison to meso-NPC, Co_2NiO_x and commercial RuO_2 (Figs. 12(e) and 12(f)), the meso-NPC/Co_2NiO_x hybrid showed enhanced OER activity with the lowest overpotential (330 mV at a current density of 10 $mA \cdot cm^{-2}$) and the smallest Tafel slope (54.0 $mV \cdot dec^{-1}$). In another attempt, Dong et al. used a template-free approach to fabricate hollow-structured Co, Fe bimetal-glycerate [126]. This Co, Fe bimetal-glycerate catalyst showed a low overpotential of 242 mV at 10 $mA \cdot cm^{-2}$ and enhanced OER kinetics with a Tafel slope of 49.4 $mV \cdot dec^{-1}$. It was shown that the appearance of oxyhydroxide-containing groups on the surface of Co, Fe bimetal-glycerate was favorable to robust OER activity. In addition, the specific hollow structure, along with the interaction between Co^{2+} and Fe^{3+}, also contributed to the OER catalytic performance.

It is well-known that active sites exposure is of great importance to catalyst performance. Excepting the well-dispersed nanoparticles, single-atom catalysts with atomically distributed metal on supports have attracted tremendous interest for their role as new frontiers in electrocatalysis due to the maximum atom-utilization efficiency [127,128]. Up until now, NC materials have been the most popular support for single-atom catalysts dispersal, as the N groups are favorable to the anchoring of metal species. As a typical example, Zhang et al. explored the role of isolated atomically dispersed Ni sites supported on NHCSs (HCM@Ni-N) as robust OER electrocatalysts in alkaline condition. The HCM@Ni-N hybrid were prepared by coating a layer of methylimidazole-Ni on the core-shell structured SiO_2@resorcinol formaldehyde [129]. X-ray absorption spectroscopy revealed that the unsaturated coordination geometry formed by the isolated Ni atoms and N atoms was the effective electronic coupling for OER. DFT results proved that Ni-N coordination could reduce the Fermi level and decrease the intermediates adsorption energy, thus significantly boosting OER kinetics. Therefore, the HCM@Ni-N has high OER activity (overpotential of 304 mV in 1.0 $mol \cdot L^{-1}$ KOH, 403 mV in 0.5 $mol \cdot L^{-1}$ H_2SO_4 to achieve 10 $mA \cdot cm^{-2}$) and excellent stability.

3.4 Water splitting

Electrochemical water splitting is recognized as a promising renewable energy conversion system. It consists of two half-cell reactions: cathodic HER and anodic OER. In theory, a cell voltage of 1.23 V is required for water electrolysis reaction, but in practice, the kinetic barriers occurring in both OER and HER processes cause a much higher operating voltage. Thus, significant efforts have been made to explore inexpensive, energy-saving, and durable bifunctional electrocatalysts.

Carbon materials that count with heteroatom doping have been shown to be efficient catalysts for both HER and OER [25,55,100]. N-doped hollow carbons with abundant pyridinic-N have been used as catalysts to effectively catalyze both HER and OER with low overpotential. To reach 10 $mA \cdot cm^{-2}$ in 1.0 $mol \cdot L^{-1}$ KOH, the required device voltage is 1.61 V [130]. Integrated transition metals and heteroatom-doped carbons have been reported as promising bifunctional catalysts for water splitting [131,132]. Pu et al. encapsulated a series of transition-metal phosphide (Fe_2P, FeP, Co_2P, CoP, etc.) nanoparticles into an NC matrix by the direct carbonization of a metal salt, $NH_4H_2PO_4$ and melamine mixture. Among these transition-metal phosphides, Ni_2P@NC required the lowest overpotential: ~138 mV to motivate HER in 0.5 $mol \cdot L^{-1}$ H_2SO_4, and ~320 mV for OER in 1.0 $mol \cdot L^{-1}$ KOH to afford 10 $mA \cdot cm^{-2}$. When Ni_2P@NC was used as both the cathode and anode for water splitting (1.0 $mol \cdot L^{-1}$ KOH), the current densities of 10 and 20 $mA \cdot cm^{-2}$ were achieved at cell voltages of 1.67 and 1.77 V, respectively. In addition, Ni_2P@NC displayed high durability for a period of 10 h in both acid and alkaline media [133].

Increased effective active sites and decreased charge transport resistance are expected to achieve enhanced electrocatalytic activity. NC nanofibers (NCF) were introduced to CoP/NHCSs (CoP/NC) as channels for a rapid charge transfer [134]. Compared with single NCF and CoP/NC, the CoP/NC/NCF hybrid catalysts exhibited promoted HER activities with low overpotential (86 mV at 10 $mA \cdot cm^{-2}$) and Tafel slope (55 $mV \cdot dec^{-1}$) in 0.5 $mol \cdot L^{-1}$ H_2SO_4, as well as superior catalytic behavior for OER with a low overpotential of 288 mV and Tafel slope of 60 $mV \cdot dec^{-1}$ in 1.0 $mol \cdot L^{-1}$ KOH. When employed in a two-electrode system (1.0 $mol \cdot L^{-1}$ KOH), a cell voltage of 1.64 V was needed in order to afford 10 $mA \cdot cm^{-2}$.

3.5 Rechargeable metal-air batteries

Metal-air batteries relying on ORR and OER, have the

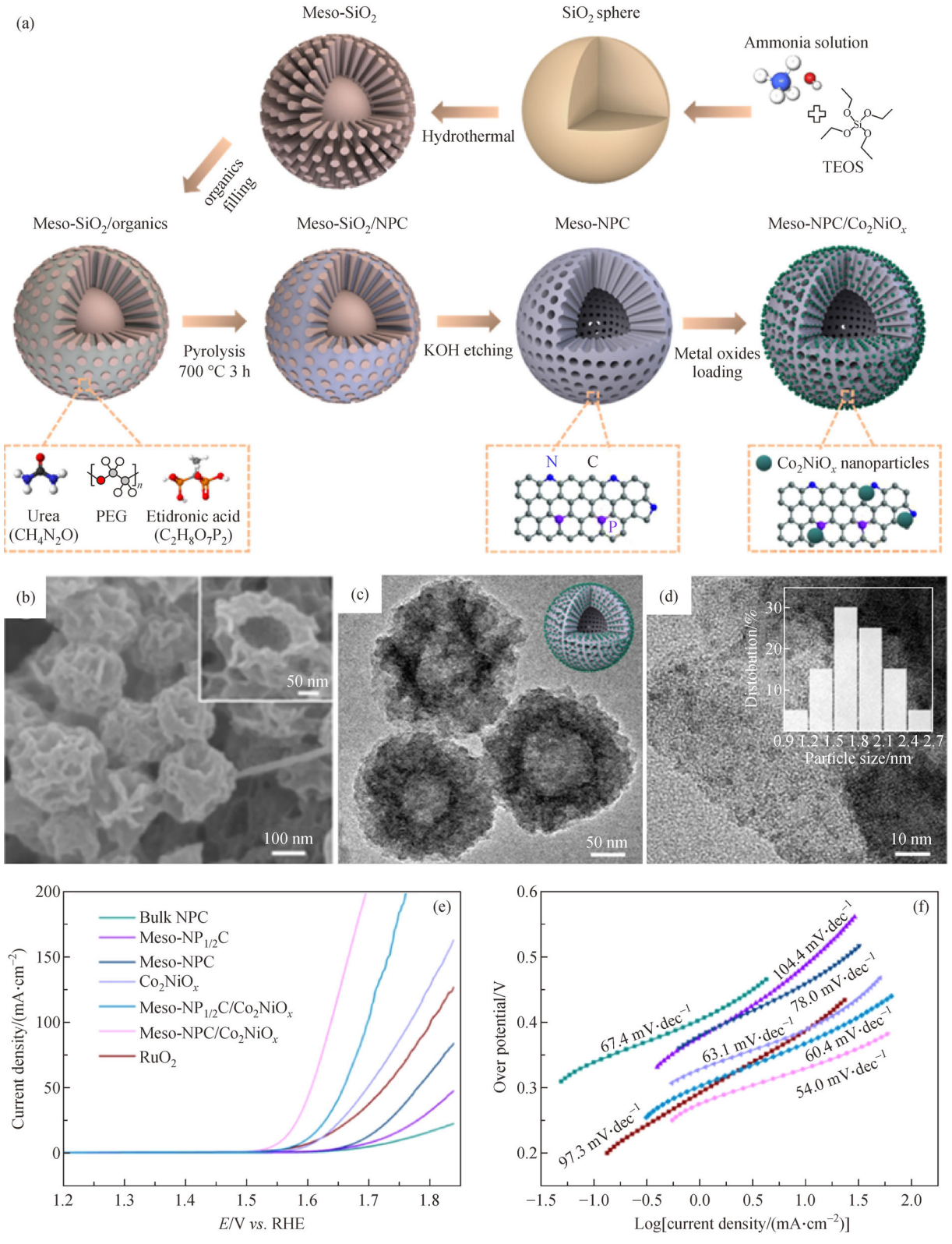

Fig. 12 (a) Schematic illustration of the Meso-NPC/Co_2NiO_x hybrid; (b) SEM images of meso-NPC; (c, d) TEM images; (e) linear sweep voltammetry curves; (f) Tafel plots of different samples in 1.0 mol·L^{-1} KOH solution. Reprinted with permission from ref. [89], copyright 2020 American Chemical Society.

advantages of being more environmentally friendly than many alternatives, and low cost, all of which make them an ideal substitute for Li batteries. Currently, Pt and Ru are the most popular advanced catalysts for ORR and OER, respectively. Both have an active catalytic effect, but are seriously limited by their high cost, low selectivity and poor cycle stability. For this reason, more promising catalytic materials, such as single, binary or ternary nonmetallic/metallic heteroatom-doped carbon [135], transition metals and transition metals-based hybrids [131,136] are being extensively developed.

Isolated single atomic sites coordinated with nitrogen on a carbon matrix (M-N-C, M = Fe, Co, Ni, Cu, etc.) have captured increasing attention due to their outstanding enhancement in catalytic activity and their stability as bifunctional ORR/OER electrocatalysts in acidic and alkaline medias [100,109,137]. The performance of M-N-C-based electrocatalysts could be promoted by introducing dual heteroatom coordinated metal centers. To test this, N and P co-coordinated Fe atoms were dispersed on the shell of the HCSs (named as FeNPC). The FeNPC exhibited enhanced activity by catalyzing ORR with an onset potential of 1.03 V and $E_{1/2}$ of 0.88 V in alkaline solution. Furthermore, the results from an in-depth simulation indicated that the quasi-octahedral O_2-FeN_xP_y species acted as active sites. They could modify the Fe electronic configuration and promote both ORR and OER processes. The FeNPC-based rechargeable Zn-air battery exhibited a high power density of 233.2 $mW \cdot cm^{-2}$ at 313.1 $mA \cdot cm^{-2}$ without any remarkable deterioration for a period of 15 h [138].

Monometallic Fe-N-C show considerable ORR and OER activity, and their catalytic performances can be further boosted by alloying with other transition metals (Ni, Cu, Pd, and Pt) [139]. In comparison to their parent metals, bimetallic alloys display some unique electronic properties by modifying the electron density around the Fermi level, which is critical for the improvement of catalytic activity. Recently, Jose et al. entrapped single atomic Fe-Co alloying in NHCSs [140]. The hollow carbon shell composed of a large amount of pores favored the transmission of mass and ion. The Fe single-atom sites adjacent to the Co site can promote O_2 adsorption on the active site of Co, meaning that it delivered a low onset/half-wave potential of 0.96/0.86 V for ORR, and a small overpotential of 360 mV at 10 $mA \cdot cm^{-2}$ for OER. When used as air cathodes for Zn-air batteries, the specific capacity and power density were 819.6 $mAh \cdot g^{-1}$ and 86.65 $mW \cdot cm^{-2}$, respectively, which is much higher than those shown by the Pt/C/RuO_2 cathode (779.7 $mAh \cdot g^{-1}$ and 110.3 $mW \cdot cm^{-2}$).

In addition to metallic and nonmetallic heteroatom co-doped carbon, the catalytic active metal oxides supported on the shells of HCSs were also demonstrated to be effective and stable bifunctional electrocatalysts for ORR and OER [100]. For this catalytic system, the hybrids take advantage of unique hollow structure and high conductivity of NHCSs, as well as high activity of metal oxides. For example, the Co_3O_4@NHCS composite catalyst exhibited reasonable bifunctional electrocatalytic activity and could therefore be adopted as an oxygen electrode for Li-O_2 batteries [141]. Fe_3O_4 is another widely investigated high-efficiency bifunctional ORR/OER electrocatalyst [91]. Fe_3O_4 nanoparticles were grown on the inner wall of NHCSs through the use of the capillary force induced melting-diffusion strategy and working as the bifunctional catalyst for ORR and OER [93]. The yolk-shell structured Fe_{20}@NHCSs catalyst exhibited excellent ORR ($E_{1/2}$ = 0.850 V) and OER (289 mV at 10 $mA \cdot cm^{-2}$) activities. The Zn-air battery equipped with Fe_{20}@N/HCSs owned a high power density of 140.8 $mW \cdot cm^{-2}$ and displayed excellent long-term stability over a 300 h period.

Transition-metal spinel oxide is another bifunctional ORR/OER electrocatalyst. Considering the relatively low electrical conductivity of transition-metal spinel oxide, it is always compounded with high-conductivity materials. Wu et al. encapsulated $MnFe_2O_4$/Fe in mesostructured NHCSs by a direct carbonization of the Fe/Mn-incorporated PDA nanosphere, and then used it as a bifunctional electrocatalyst for ORR and OER in alkaline condition [142]. These hybrids displayed synergistically improved ORR/OER activity. When used as a Zn-air battery electrode, the maximum power density was 37 $mW \cdot cm^{-2}$, much higher than that of a Pt/C-based battery (28 $mW \cdot cm^{-2}$).

3.6 Pollutant degradation

Over the past few decades, the presence of toxic pollutants (e.g., phenol, bisphenol A, antibiotics, heavy metal ion) in aquatic environments have led to serious environmental pollution and possible negative influences on human health. The removal of pollutants from contaminated water is therefore an urgent issue. Photocatalysis is regarded as a type of ecofriendly technology for the effective removal of both organic and inorganic pollutants [143,144].

For photocatalysts, it is well-known that absorption of visible-light, efficiency of electron-hole separation and charge migration rate are all crucial factors for the improvement of photocatalysis efficiency [144]. N-doped hollow mesoporous carbon spheres (N-HMCs) and g-C_3N_4/Bi_2O_3 were combined together to achieve an effective photocatalytic system for the photodegradation of antibiotics under visible-light. The synergistic actions of g-C_3N_4/Bi_2O_3 and N-HMCs, and especially the presence of N-HMCs, were indispensable for the improvement of photocatalytic efficiency. To be specific, N-HMCs could serve as photosensitizers to enhance visible-light absorption, and also as conductive materials for the transformation of photoexcited electrons [145]. g-C_3N_4/CdS-NHCs

hybrids are also regarded as a good photocatalytic catalyst, showing high efficiency and stability for cloxacillin degradation [146].

Cr(VI) and phenols (phenol and bisphenol A) have also gained increased attention recently because of their acute toxicity and potential carcinogenicity [147]. Current research has combined adsorption and degradation processes to realize a maximum removal of these pollutants. For instance, sheet-like $ZnIn_2S_4$ grown on NHCSs has been shown to be an effective photocatalyst for the reduction of Cr(VI). The favorable band gap and excellent electrical conductivity of $ZnIn_2S_4$ leads to the hybrids having a superior light-driven photocatalytic efficiency and an excellent degradation rate for aqueous Cr(VI) [148]. Meanwhile, MnO_2 was incorporated into NHCSs (MnO_2@NHCSs) and used for the adsorption and degradation of bisphenol A. Owing to the oxidation properties of MnO_2 and its unique hollow structure, MnO_2@NHCSs was able to completely degrade bisphenol A to H_2O and CO_2 (99.6%) within 30 min [149]. Some other heterojunctions, such as Fe_3O_4-CuO@HCSs, illustrated a superb photocatalytic performance for the degradation of bisphenol A under visible light [88].

Excepting photocatalysis, advanced oxidation processes are another excellent solution for the removal of organic compounds from water. Cu-Co/NHCSs synthesized through pyrolysis polystyrene spheres@ZIF-67, showed high activity for 4-nitrophenol decomposition. Moreover, this catalyst was convenient for magnetic recovery, and after being reused five times, it still maintained a good catalytic performance [150].

4 Conclusions and outlook

In summary, significant progress has been made toward achieving an adjustable surface chemistry, porous structure and hybrid architecture in HCSs. This review article has demonstrated the development in the synthesis and functionalization of HCSs, and their noble-metal free hybrids in catalysis. The porous structure in the carbon shell and its morphology are two of the most important textual properties of HCSs. Their synthesis can be controlled by selecting/adjusting specific hard/soft templates or solvents. Functionalization of HCSs is mainly operated in two ways: one introduces one or more heteroatoms (N, S, P, B) into the carbon skeleton through heteroatom-containing carbon precursors, catalysts and templates; and the other way is to construct hybrid architectures by assembling HCSs with metal-free/containing species, such as graphene, CNTs, metal oxide, and metal sulfide. The large surface area and hollow cores enable a homogeneous distribution of the active species, and short transport pathways. In addition, the high conductivity, as well as the chemical stability of HCSs favor long-time catalytic stability. All these merits guide an improved catalytic performance for ORR, HER and pollution degradation.

Although great progress has been made, work remains to be done on the synthesis of HCSs with controllable structures and certain compositions in a controlled manner, as well as on their application possibilities. Currently, most reported hollow-structured carbon spheres appear with a diameter of several hundred nanometers. Considering the reaction kinetics of guest molecule releasing, monodispersed HCSs with a particle size of less than 100 nm are attractive. Finding a way to easily fabricate nano-sized HCSs with high dispersity remains a great challenge. Another issues is that the employed hard templates are mainly formed of silica, polystyrene and PMMA spheres. Therefore, finding new types of polymeric template, especially one with abundant heteroatoms and that can easily be removed through carbonization, is of interest to the area of carbon synthesis. Another issue is posed by the incorporation of guest substances into the inner wall of HCSs. Although this is always carried out through a capillary effect, the loading amount remains far from satisfactory. To solve this, active materials can be deposited onto the surface of HCSs shell to realize higher loading, and in addition, this might be further promoted through the development of multi-shell structures.

Hollow-structured carbon-based electro/photocatalysts have gained significant attention. This is due to their hollow interiors and porous shells providing more available space for the exposure of abundant active sites and promotion of mass transport. They show great potential for ORR, HER and OER in various electrochemical processes, such as in water splitting and rechargeable metal-air batteries. For metal-free HCSs, heteroatom-doping can modulate the electronic structures and provide active sites to catalyze the ORR, HER and OER processes. Encapsulating or supporting the catalytic active species from the nanoparticles to single-site atoms into the HCSs configurations has proven to be an effective way to design advanced catalysts. In addition, hybridizing HCSs with transition metal-based catalysts is expected to create more active sites, as well as generate high adsorption abilities for the reactive intermediates. Although great progress has been made, the catalytic performance of HCSs-based electrocatalysts is still incompatible with nobel-metal based catalysts. An engineering of electrocatalysts for improved ORR/HER/OER catalytic activity is thus highly required.

Rational design of bifunctional ORR/OER and HER/OER catalysts is conducive to the promotion of energy conversion and storage devices (i.e., water splitting, rechargeable metal-air batteries). However, it is still not easy for catalysts to possess ORR/OER or HER/OER activity simultaneously. As far as we know, Fe-based catalysts (Fe-C-N, Fe_3O_4) and transition-metal phosphides account for a large proportion of the active materials anchoring on HCSs in metal-air batteries and water

splitting, respectively. Considering the controllable structure/morphology of those HCSs equipped with abundant exposed active sites, some other transition metal-based catalysts should be concerned with constructing a highly active hybrid structure. Moreover, in order to make full use of the HCSs' voids, a deposition/impregnation of active nanomaterials onto both the inner and outer sides of the carbon shell is highly effective. Efficient and controllable encapsulating methods are highly desired. The fabrication of multishell-structured HCSs and regulation of its porous structure and surface properties is expected to increase the interaction between active materials and HCSs.

As a half-reaction for both water splitting and metal-air batteries, the activity of OER is of great importance. However, OER electrocatalysts are limited to basic solutions, and in addition, their long-term stability is less than satisfactory. Effective and stable bifunctional electrocatalysts in a wide pH range would be beneficial for the catalysts during practical application. Therefore, future research should be devoted to designing HCS-based electrocatalysts to catalyze ORR/HER/OER at a low overpotential and a wide pH range.

Modeling and/or simulation methods have been used to understand the catalytic activity and mechanisms, and further guide the construction of the desired electronic structure. The scaling relationships of the synergistic effect between metals, or metal and carbons, to the electrochemical performances have not yet been realized. Moreover, although carbon support can improve the stability of HCSs-based electrocatalysts, their degradation mechanism still lacks understanding. In conclusion, research on HCS-derived electro/photocatalysts is only just beginning. In order to achieve an in-depth understanding of the active sites, corresponding catalytic mechanisms, and the structure-activity relationships, on-going and further investigations are still required. It is also necessary to provide opportunities for their applications in other reaction systems.

Acknowledgements This work was supported by Natural Science Foundation of Shandong province (Grant No. ZR2019QEM005). Project of Shandong province Higher Educational Young Innovative Talent Introduction and Cultivation Team [environmental functional material innovation team] and the SDUST Research Fund (Grant No. 2015YQJH101).

References

1. Ding J, Zhang H, Zhou H, Feng J, Zheng X, Zhong C, Paek E, Hu W, Mitlin D. Sulfur-grafted hollow carbon spheres for potassium-ion battery anodes. Advanced Materials, 2019, 31(30): 1900429
2. Zhang Y, He Z, Wang H, Qi L, Liu G, Zhang X. Applications of hollow nanomaterials in environmental remediation and monitoring: A review. Frontiers of Chemical Science and Engineering, 2015, 9(5): 770–783
3. Cheng Y, Li Z, Li Y, Dai S, Ji G, Zhao H, Cao J, Du Y. Rationally regulating complex dielectric parameters of mesoporous carbon hollow spheres to carry out efficient microwave absorption. Carbon, 2018, 127: 643–652
4. Han Y, Wang Y G, Chen W, Xu R, Zheng L, Zhang J, Luo J, Shen R A, Zhu Y, Cheong W C, et al. Hollow N-doped carbon spheres with isolated cobalt single atomic sites: superior electrocatalysts for oxygen reduction. Journal of the American Chemical Society, 2017, 139(48): 17269–17272
5. Xu M, Liu Y, Yu Q, Feng S, Zhou L, Mai L. Phenylenediamine-formaldehyde chemistry derived N-doped hollow carbon spheres for high-energy-density supercapacitors. Chinese Chemical Letters, 2021, 32(1): 184–189
6. Yan C, Meng N, Lyu W, Li Y, Wang L, Liao Y. Hierarchical porous hollow carbon spheres derived from spirofluorene-and aniline-linked conjugated microporous polymer for phase change energy storage. Carbon, 2021, 176: 178–187
7. Du J, Chen A, Liu L, Li B, Zhang Y. N-doped hollow mesoporous carbon spheres prepared by polybenzoxazines precursor for energy storage. Carbon, 2020, 160: 265–272
8. Pei F, An T, Zang J, Zhao X, Fang X, Zheng M, Dong Q, Zheng N. From hollow carbon spheres to N-doped hollow porous carbon bowls: rational design of hollow carbon host for Li-S batteries. Advanced Energy Materials, 2016, 6(8): 1502539
9. Ye C, Zhang L, Guo C, Li D, Vasileff A, Wang H, Qiao S Z. A 3D hybrid of chemically coupled nickel sulfide and hollow carbon spheres for high performance lithium-sulfur batteries. Advanced Functional Materials, 2017, 27(33): 1702524
10. Niu H, Zhang Y, Liu Y, Luo B, Xin N, Shi W. MOFs-derived Co_9S_8-embedded graphene/hollow carbon spheres film with macroporous frameworks for hybrid supercapacitors with superior volumetric energy density. Journal of Materials Chemistry. A, Materials for Energy and Sustainability, 2019, 7(14): 8503–8509
11. Zheng W, Yang J, Chen H, Hou Y, Wang Q, Gu M, He F, Xia Y, Xia Z, Li Z, et al. Atomically defined undercoordinated active sites for highly efficient CO_2 electroreduction. Advanced Functional Materials, 2019, 30(4): 1907658
12. Lei C, Zheng Q, Cheng F, Hou Y, Yang B, Li Z, Wen Z, Lei L, Chai G, Feng X. High-performance metal-free nanosheets array electrocatalyst for oxygen evolution reaction in acid. Advanced Functional Materials, 2020, 30(31): 2003000
13. Wang T, Sang X, Zheng W, Yang B, Yao S, Lei C, Li Z, He Q, Lu J, Lei L, et al. Gas diffusion strategy for inserting atomic iron sites into graphitized carbon supports for unusually high-efficient CO_2 electroreduction and high-performance Zn-CO_2 batteries. Advanced Materials, 2020, 32(29): 2002430
14. Li Y, Li J, Huang J, Chen J, Kong Y, Yang B, Li Z, Lei L, Chai G, Wen Z, et al. Boosting electroreduction kinetics of nitrogen to ammonia via tuning electron distribution of single-atomic iron sites. Angewandte Chemie International Edition, 2021, 60(16): 9078–9085
15. Wang X, Wang Y, Sang X, Zheng W, Zhang S, Shuai L, Yang B, Li Z, Chen J, Lei L, et al. Dynamic activation of adsorbed intermediates via axial traction for the promoted electrochemical CO_2 reduction. Angewandte Chemie International Edition, 2021, 60(8): 4192–4198

16. Zheng W, Wang Y, Shuai L, Wang X, He F, Lei C, Li Z, Yang B, Lei L, Yuan C, et al. Highly boosted reaction kinetics in carbon dioxide electroreduction by surface-introduced electronegative dopants. Advanced Functional Materials, 2021, 31(15): 2008146
17. Li S, Pasc A, Fierro V, Celzard A. Hollow carbon spheres, synthesis and applications—a review. Journal of Materials Chemistry. A, Materials for Energy and Sustainability, 2016, 4(33): 12686–12713
18. Liu T, Zhang L, Cheng B, Yu J. Hollow carbon spheres and their hybrid nanomaterials in electrochemical energy storage. Advanced Energy Materials, 2019, 9(17): 1803900
19. Yang J, Han H, Repich H, Zhi R, Qu C, Kong L, Kaskel S, Wang H, Xu F, Li H. Recent progress on the design of hollow carbon spheres to host sulfur in room-temperature sodium-sulfur batteries. New Carbon Materials, 2020, 35(6): 630–645
20. Jiang J, Nie G, Nie P, Li Z, Pan Z, Kou Z, Dou H, Zhang X, Wang J. Nanohollow carbon for rechargeable batteries: ongoing progresses and challenges. Nano-Micro Letters, 2020, 12(1): 183
21. Zhang Y, Sun K, Zhan L, Wang Y, Ling L. N-doped yolk-shell hollow carbon sphere wrapped with graphene as sulfur host for high-performance lithium-sulfur batteries. Applied Surface Science, 2018, 427: 823–829
22. Zhang Y, Ma Q, Wang S, Liu X, Li L. Poly(vinyl alcohol)-assisted fabrication of hollow carbon spheres/reduced graphene oxide nanocomposites for high-performance lithium-ion battery anodes. ACS Nano, 2018, 12(5): 4824–4834
23. Zhang S L, Guan B Y, Lou X W. Co-Fe alloy/N-doped carbon hollow spheres derived from dual metal-organic frameworks for enhanced electrocatalytic oxygen reduction. Small, 2019, 15(13): 1805324
24. Du J, Liu L, Yu Y, Hu Z, Zhang Y, Liu B, Chen A. Tuning confined nanospace for preparation of N-doped hollow carbon spheres for high performance supercapacitors. ChemSusChem, 2019, 12(1): 303–309
25. Hassan M, Qiu W, Song X, Mao Q, Ren S, Hao C. Supercapacitive and ORR performances of nitrogen-doped hollow carbon spheres pyrolyzed from polystyrene@polypyrrole-polyaniline. Journal of Alloys and Compounds, 2020, 818: 152890
26. Fan D, Wei B, Wu R, Zhou J, Zhou C. Dielectric control of ultralight hollow porous carbon spheres and excellent microwave absorbing properties. Journal of Materials Science, 2021, 56(11): 6830–6844
27. Fang X, Liu S, Zang J, Xu C, Zheng M S, Dong Q F, Sun D, Zheng N. Precisely controlled resorcinol-formaldehyde resin coating for fabricating core-shell, hollow, and yolk-shell carbon nanostructures. Nanoscale, 2013, 5(15): 6908–6916
28. Liu M, Yu Y, Liu B, Liu L, Lv H, Chen A. PVP-assisted synthesis of nitrogen-doped hollow carbon spheres for supercapacitors. Journal of Alloys and Compounds, 2018, 768: 42–48
29. Bu L, Kuai X, Zhu W, Kai X, Lu T, Zhao J, Gao L. Nitrogen-doped double-shell hollow carbon spheres for fast and stable sodium ion storage. Electrochimica Acta, 2020, 356: 136804
30. Han J, Xu G, Ding B, Pan J, Dou H, MacFarlane D R. Porous nitrogen-doped hollow carbon spheres derived from polyaniline for high performance supercapacitors. Journal of Materials Chemistry. A, Materials for Energy and Sustainability, 2014, 2(15): 5352–5357
31. Gil-Herrera L K, Blanco Á, Juárez B H, López C. Seeded synthesis of monodisperse core-shell and hollow carbon spheres. Small, 2016, 12(32): 4357–4362
32. Yang X, Li Y, Zhang P, Sun L, Ren X, Mi H. Hierarchical hollow carbon spheres: novel synthesis strategy, pore structure engineering and application for micro-supercapacitor. Carbon, 2020, 157: 70–79
33. He M, Jia J, Sun Q, Zhang W. Hollow N-doped carbon sphere synthesized by MOF as superior oxygen electrocatalyst for Li-O_2 batteries. International Journal of Energy Research, 2020, 45(5): 7120–7128
34. Liu L, Xu S D, Yu Q, Wang F Y, Zhu H L, Zhang R L, Liu X. Nitrogen-doped hollow carbon spheres with a wrinkled surface: their one-pot carbonization synthesis and supercapacitor properties. Chemical Communications, 2016, 52(78): 11693–11696
35. Liu F, Yuan R L, Zhang N, Ke C C, Ma S X, Zhang R L, Liu L. Solvent-induced synthesis of nitrogen-doped hollow carbon spheres with tunable surface morphology for supercapacitors. Applied Surface Science, 2018, 437: 271–280
36. He X, Sun H, Zhu M, Yaseen M, Liao D, Cui X, Guan H, Tong Z, Zhao Z. N-Doped porous graphitic carbon with multi-flaky shell hollow structure prepared using a green and 'useful' template of $CaCO_3$ for VOC fast adsorption and small peptide enrichment. Chemical Communications, 2017, 53(24): 3442–3445
37. Guo H, Ding B, Wang J, Zhang Y, Hao X, Wu L, An Y, Dou H, Zhang X. Template-induced self-activation route for nitrogen-doped hierarchically porous carbon spheres for electric double layer capacitors. Carbon, 2018, 136: 204–210
38. Du W, Wang X, Zhan J, Sun X, Kang L, Jiang F, Zhang X, Shao Q, Dong M, Liu H, et al. Biological cell template synthesis of nitrogen-doped porous hollow carbon spheres/MnO_2 composites for high-performance asymmetric supercapacitors. Electrochimica Acta, 2019, 296: 907–915
39. Tang Y, Wang X, Chen J, Wang X, Wang D, Mao Z. Templated transformation of g-C_3N_4 nanosheets into nitrogen-doped hollow carbon sphere with tunable nitrogen-doping properties for application in Li-ions batteries. Carbon, 2020, 168: 458–467
40. Zhang D, Shen S, Xiao X, Mao D, Yan B. Nitrogen-doped hollow carbon spheres with tunable shell thickness for high-performance supercapacitors. RSC Advances, 2020, 10(44): 26546–26552
41. Xu T, Wang Q, Zhang J, Xie X, Xia B. Green synthesis of dual carbon conductive network-encapsulated hollow SiO_x spheres for superior lithium-ion batteries. ACS Applied Materials & Interfaces, 2019, 11(22): 19959–19967
42. Yang Z C, Zhang Y, Kong J H, Wong S Y, Li X, Wang J. Hollow carbon nanoparticles of tunable size and wall thickness by hydrothermal treatment of α-cyclodextrin templated by F127 block copolymers. Chemistry of Materials, 2013, 25(5): 704–710
43. Li W, Li B, Shen M, Gao Q, Hou J. Use of Gemini surfactant as emulsion interface microreactor for the synthesis of nitrogen-doped hollow carbon spheres for high-performance supercapacitors. Chemical Engineering Journal, 2020, 384: 123309
44. Sun H, Zhu Y, Yang B, Wang Y, Wu Y, Du J. Template-free

fabrication of nitrogen-doped hollow carbon spheres for high-performance supercapacitors based on a scalable homopolymer vesicle. Journal of Materials Chemistry. A, Materials for Energy and Sustainability, 2016, 4(31): 12088–12097

45. Huang X, Zhang T, Asefa T. Hollow mesoporous carbon microparticles and micromotors with single holes templated by colloidal silica-assisted gas bubbles. Small, 2017, 13(26): 1700256
46. Liu X, Song P, Hou J, Wang B, Xu F, Zhang X. Revealing the dynamic formation process and mechanism of hollow carbon spheres: from bowl to sphere. ACS Sustainable Chemistry & Engineering, 2018, 6(2): 2797–2805
47. Liu D, Xue N, Wei L, Zhang Y, Qin Z, Li X, Binks B P, Yang H. Surfactant assembly within pickering emulsion droplets for fabrication of interior-structured mesoporous carbon microspheres. Angewandte Chemie International Edition, 2018, 57(34): 10899–10904
48. Chen M, Su Z, Liu Y, Pan Y, Zhang Y, Hu M, Ma Q, Zhou Q, Long D. Self-propelled nanoemulsion assembly of organosilane to the synthesis of high-surface-area hollow carbon spheres for enhanced energy storage. Chemical Engineering Journal, 2020, 400: 124973
49. Wang K, Huang L, Razzaque S, Jin S, Tan B. Fabrication of hollow microporous carbon spheres from hyper-crosslinked microporous polymers. Small, 2016, 12(23): 3134–3142
50. Wang S, Sun W, Yang D S, Yang F. Conversion of soybean waste to sub-micron porous-hollow carbon spheres for supercapacitor via a reagent and template-free route. Materials Today. Energy, 2019, 13: 50–55
51. Yang Y, Jin S, Zhang Z, Du Z, Liu H, Yang J, Xu H, Ji H. Nitrogen-doped hollow carbon nanospheres for high-performance Li-ion batteries. ACS Applied Materials & Interfaces, 2017, 9(16): 14180–14186
52. Shang M, Zhang J, Liu X, Liu Y, Guo S, Yu S, Filatov S, Yi X N. S self-doped hollow-sphere porous carbon derived from puffball spores for high performance supercapacitors. Applied Surface Science, 2021, 542: 148697
53. Zhang L, Liu L, Liu M, Yu Y, Hu Z, Liu B, Lv H, Chen A. Controllable synthesis of N-doped hollow, yolk-shell and solid carbon spheres via template-free method. Journal of Alloys and Compounds, 2019, 778: 294–301
54. Zhou J, Sun Z, Chen M, Wang J, Qiao W, Long D, Ling L. Macroscopic and mechanically robust hollow carbon spheres with superior oil adsorption and light-to-heat evaporation properties. Advanced Functional Materials, 2016, 26(29): 5368–5375
55. Guan B Y, Zhang S L, Lou X W D. Realization of walnut-shaped particles with macro-/mesoporous open channels through pore architecture manipulation and their use in electrocatalytic oxygen reduction. Angewandte Chemie International Edition, 2018, 57(21): 6176–6180
56. Du J, Liu L, Wu H, Lv H, Chen A. Tunable N-doped hollow carbon spheres induced by an ionic liquid for energy storage applications. Materials Chemistry Frontiers, 2020, 5(2): 843–850
57. Liu P, Liu W, Huang Y, Li P, Yan J, Liu K. Mesoporous hollow carbon spheres boosted, integrated high performance aqueous Zn-ion energy storage. Energy Storage Materials, 2020, 25: 858–865
58. Xu F, Tang Z, Huang S, Chen L, Liang Y, Mai W, Zhong H, Fu R, Wu D. Facile synthesis of ultrahigh-surface-area hollow carbon nanospheres for enhanced adsorption and energy storage. Nature Communications, 2015, 6(1): 7221
59. Tang J, Liu J, Salunkhe R R, Wang T, Yamauchi Y. Nitrogen-doped hollow carbon spheres with large mesoporous shells engineered from diblock copolymer micelles. Chemical Communications, 2016, 52(3): 505–508
60. Fang M, Chen Z, Tian Q, Cao Y, Wang C, Liu Y, Fu J, Zhang J, Zhu L, Yang C, Chen J, Xu Q. Synthesis of uniform discrete cage-like nitrogen-doped hollow porous carbon spheres with tunable direct large mesoporous for ultrahigh supercapacitive performance. Applied Surface Science, 2017, 425: 69–76
61. Qiao Z A, Guo B, Binder A J, Chen J, Veith G M, Dai S. Controlled synthesis of mesoporous carbon nanostructures via a "silica-assisted" strategy. Nano Letters, 2013, 13(1): 207–212
62. Zhang H, Noonan O, Huang X, Yang Y, Xu C, Zhou L, Yu C. Surfactant-free assembly of mesoporous carbon hollow spheres with large tunable pore sizes. ACS Nano, 2016, 10(4): 4579–4586
63. Cheng Y, Zhao H, Zhao Y, Cao J, Zheng J, Ji G. Structure-switchable mesoporous carbon hollow sphere framework toward sensitive microwave response. Carbon, 2020, 161: 870–879
64. Zhang N, Liu F, Xu S D, Wang F Y, Yu Q, Liu L. Nitrogen-phosphorus co-doped hollow carbon microspheres with hierarchical micro-meso-macroporous shells as efficient electrodes for supercapacitors. Journal of Materials Chemistry. A, Materials for Energy and Sustainability, 2017, 5(43): 22631–22640
65. Du J, Zhang Y, Wu H, Hou S, Chen A. N-doped hollow mesoporous carbon spheres by improved dissolution-capture for supercapacitors. Carbon, 2020, 156: 523–528
66. Shang Y, Hu X, Li X, Cai S, Liang G, Zhao J, Zheng C, Sun X. A facile synthesis of nitrogen-doped hierarchical porous carbon with hollow sphere structure for high-performance supercapacitors. Journal of Materials Science, 2019, 54(19): 12747–12757
67. Wang C, Wang F, Liu Z, Zhao Y, Liu Y, Yue Q, Zhu H, Deng Y, Wu Y, Zhao D. N-doped carbon hollow microspheres for metal-free quasi-solid-state full sodium-ion capacitors. Nano Energy, 2017, 41: 674–680
68. Tetana Z, Mhlanga S, Coville N. Chemical vapour deposition syntheses and characterization of boron-doped hollow carbon spheres. Diamond and Related Materials, 2017, 74: 70–80
69. Ravat V, Nongwe I, Meijboom R, Bepete G, Coville N J. Pd on boron-doped hollow carbon spheres-PdO particle size and support effects. Journal of Catalysis, 2013, 305: 36–45
70. Wu J, Jin C, Yang Z, Tian J, Yang R. Synthesis of phosphorus-doped carbon hollow spheres as efficient metal-free electrocatalysts for oxygen reduction. Carbon, 2015, 82: 562–571
71. Ni D, Sun W, Wang Z, Bai Y, Lei H, Lai X, Sun K. Heteroatom-doped mesoporous hollow carbon spheres for fast sodium storage with an ultralong cycle life. Advanced Energy Materials, 2019, 9(19): 1900036
72. Ke C C, Zhang N, Liu F, Yu Q, Wang F Y, Liu L, Zhang R L, Liu X, Zeng R C. Deflated balloon-like nitrogen-rich sulfur-containing hierarchical porous carbons for high-rate supercapacitors. Applied Surface Science, 2019, 484: 716–725

73. Lv B, Li P, Liu Y, Lin S, Gao B, Lin B. Nitrogen and phosphorus co-doped carbon hollow spheres derived from polypyrrole for high-performance supercapacitor electrodes. Applied Surface Science, 2018, 437: 169–175
74. Wang H, Lan J L, Yuan H, Luo S, Huang Y, Yu Y, Cai Q, Yang X. Chemical grafting-derived N,P co-doped hollow microporous carbon spheres for high-performance sodium-ion battery anodes. Applied Surface Science, 2020, 518: 146221
75. Song L, Xin S, Xu D W, Li H Q, Cong H P, Yu S H. Graphene-wrapped graphitic carbon hollow spheres: bioinspired synthesis and applications in batteries and supercapacitors. ChemNanoMat : Chemistry of Nanomaterials for Energy, Biology and More, 2016, 2(6): 540–546
76. Wang H, Shi L, Yan T, Zhang J, Zhong Q, Zhang D. Design of graphene-coated hollow mesoporous carbon spheres as high performance electrodes for capacitive deionization. Journal of Materials Chemistry. A, Materials for Energy and Sustainability, 2014, 2(13): 4739–4750
77. Shen Z, Du J, Mo Y, Chen A. Nanocomposites of reduced graphene oxide modified with mesoporous carbon layers anchored by hollow carbon spheres for energy storage. Carbon, 2021, 173: 22–30
78. Li M, Zhang Y, Yang L, Liu Y, Yao J. Hollow melamine resin-based carbon spheres/graphene composite with excellent performance for supercapacitors. Electrochimica Acta, 2015, 166: 310–319
79. Dong D, Guo H, Li G, Yan L, Zhang X, Song W. Assembling hollow carbon sphere-graphene polylithic aerogels for thermoelectric cells. Nano Energy, 2017, 39: 470–477
80. Wang Q, Yan J, Wang Y, Ning G, Fan Z, Wei T, Cheng J, Zhang M, Jing X. Template synthesis of hollow carbon spheres anchored on carbon nanotubes for high rate performance supercapacitors. Carbon, 2013, 52: 209–218
81. Chen Z, Ye S, Evans S D, Ge Y, Zhu Z, Tu Y, Yang X. Confined assembly of hollow carbon spheres in carbonaceous nanotube: a spheres-in-tube carbon nanostructure with hierarchical porosity for high-performance supercapacitor. Small, 2018, 14(19): 1704015
82. Peng Z, Wang H, Zhou L, Wang Y, Gao J, Liu G, Redfern S A, Feng X, Lu S, Li B, Liu Z. Hollow carbon shells enhanced by confined ruthenium as cost-efficient and superior catalysts for the alkaline hydrogen evolution reaction. Journal of Materials Chemistry. A, Materials for Energy and Sustainability, 2019, 7(12): 6676–6685
83. Shen J, Wu H, Sun W, Qiao J, Cai H, Wang Z, Sun K. *In-situ* nitrogen-doped hierarchical porous hollow carbon spheres anchored with iridium nanoparticles as efficient cathode catalysts for reversible lithium-oxygen batteries. Chemical Engineering Journal, 2019, 358: 340–350
84. Ma S, Wang L, Wang Y, Zuo P, He M, Zhang H, Ma L, Wu T, Yin G. Palladium nanocrystals-imbedded mesoporous hollow carbon spheres with enhanced electrochemical kinetics for high performance lithium sulfur batteries. Carbon, 2019, 143: 878–889
85. Yang G, Kuwahara Y, Masuda S, Mori K, Louis C, Yamashita H. PdAg nanoparticles and aminopolymer confined within mesoporous hollow carbon spheres as an efficient catalyst for hydrogenation of CO_2 to formate. Journal of Materials Chemistry. A, Materials for Energy and Sustainability, 2020, 8(8): 4437–4446
86. Yang G, Kuwahara Y, Mori K, Louis C, Yamashita H. PdAg alloy nanoparticles encapsulated in N-doped microporous hollow carbon spheres for hydrogenation of CO_2 to formate. Applied Catalysis B: Environmental, 2021, 283: 119628
87. Ma Y, Luo S, Tian M, Lu J, Peng Y, Desmond C, Liu Q, Li Q, Min Y, Xu Q, Chen S. Hollow carbon spheres codoped with nitrogen and iron as effective electrocatalysts for oxygen reduction reaction. Journal of Power Sources, 2020, 450: 227659
88. Qin L, Ru R, Mao J, Meng Q, Fan Z, Li X, Zhang G. Assembly of MOFs/polymer hydrogel derived Fe_3O_4-CuO@hollow carbon spheres for photochemical oxidation: freezing replacement for structural adjustment. Applied Catalysis B: Environmental, 2020, 269: 118754
89. Wang J, Zeng H C. Hybrid OER electrocatalyst combining mesoporous hollow spheres of N, P-doped carbon with ultrafine Co_2NiO_x. ACS Applied Materials & Interfaces, 2020, 12(45): 50324–50332
90. Liu T, Zhang L, You W, Yu J. Core-shell nitrogen-doped carbon hollow spheres/Co_3O_4 nanosheets as advanced electrode for high-performance supercapacitor. Small, 2018, 14(12): 1702407
91. Li Y, Huang H, Chen S, Yu X, Wang C, Ma T. 2D nanoplate assembled nitrogen doped hollow carbon sphere decorated with Fe_3O_4 as an efficient electrocatalyst for oxygen reduction reaction and Zn-air batteries. Nano Research, 2019, 12(11): 2774–2780
92. Hao R, Ren J T, Lv X W, Li W, Liu Y P, Yuan Z Y. N-doped porous carbon hollow microspheres encapsulated with iron-based nanocomposites as advanced bifunctional catalysts for rechargeable Zn-air battery. Journal of Energy Chemistry, 2020, 49: 14–21
93. Wang B, Ye Y, Xu L, Quan Y, Wei W, Zhu W, Li H, Xia J. Space-confined yolk-shell construction of Fe_3O_4 nanoparticles inside N-Doped hollow mesoporous carbon spheres as bifunctional electrocatalysts for long-term rechargeable Zinc-air batteries. Advanced Functional Materials, 2020, 30(51): 2005834
94. Pang Y, Wang K, Xie H, Sun Y, Titirici M M, Chai G L. Mesoporous carbon hollow spheres as efficient electrocatalysts for oxygen reduction to hydrogen peroxide in neutral electrolytes. ACS Catalysis, 2020, 10(14): 7434–7442
95. Zhao H, Zhu Y P, Ge L, Yuan Z Y. Nitrogen and sulfur co-doped mesoporous hollow carbon microspheres for highly efficient oxygen reduction electrocatalysts. International Journal of Hydrogen Energy, 2017, 42(30): 19010–19018
96. Lei C, Wang Y, Hou Y, Liu P, Yang J, Zhang T, Zhuang X, Chen M, Yang B, Lei L. Efficient alkaline hydrogen evolution on atomically dispersed Ni-N_x species anchored porous carbon with embedded Ni nanoparticles by accelerating water dissociation kinetics. Energy & Environmental Science, 2019, 12(1): 149–156
97. Zhao H, Yuan Z Y. Design strategies of non-noble metal-based electrocatalysts for two-electron oxygen reduction to hydrogen peroxide. ChemSusChem, 2021, 14(7): 1616–1633
98. Zhao H, Weng C C, Ren J T, Ge L, Liu Y P, Yuan Z Y. Phosphonate-derived nitrogen-doped cobalt phosphate/carbon nanotube hybrids as highly active oxygen reduction reaction electrocatalysts. Chinese Journal of Catalysis, 2020, 41(2): 259–

267

99. Zhang C, Lu C, Bi S, Hou Y, Zhang F, Cai M, He Y, Paasch S, Feng X, Brunner E, et al. S-enriched porous polymer derived N-doped porous carbons for electrochemical energy storage and conversion. Frontiers of Chemical Science and Engineering, 2018, 12(3): 346–357
100. Zeng K, Zheng X, Li C, Yan J, Tian J H, Jin C, Strasser P, Yang R. Recent advances in non-noble bifunctional oxygen electrocatalysts toward large-scale production. Advanced Functional Materials, 2020, 30(27): 2000503
101. Xiong W, Li H, Cao R. Nitrogen and sulfur dual-doped hollow mesoporous carbon spheres as efficient metal-free catalyst for oxygen reduction reaction. Inorganic Chemistry Communications, 2020, 114: 107848
102. Chen G, Liu J, Li Q, Guan P, Yu X, Xing L, Zhang J, Che R. A direct H_2O_2 production based on hollow porous carbon sphere-sulfur nanocrystal composites by confinement effect as oxygen reduction electrocatalysts. Nano Research, 2019, 12(10): 2614–2622
103. Jia N, Yang T, Shi S, Chen X, An Z, Chen Y, Yin S, Chen P N. F-codoped carbon nanocages: an efficient electrocatalyst for hydrogen peroxide electroproduction in alkaline and acidic solutions. ACS Sustainable Chemistry & Engineering, 2020, 8(7): 2883–2891
104. Dang X, Yang R, Wang Z, Wu S, Zhao H. Efficient visible-light activation of molecular oxygen to produce hydrogen peroxide using P doped g-C_3N_4 hollow spheres. Journal of Materials Chemistry. A, Materials for Energy and Sustainability, 2020, 8(43): 22720–22727
105. Hu S, Qu X, Li P, Wang F, Li Q, Song L, Zhao Y, Kang X. Photocatalytic oxygen reduction to hydrogen peroxide over copper doped graphitic carbon nitride hollow microsphere: the effect of Cu (I)-N active sites. Chemical Engineering Journal, 2018, 334: 410–418
106. Duraisamy V, Krishnan R, Senthil Kumar S M. N-doped hollow mesoporous carbon nanospheres for oxygen reduction reaction in alkaline media. ACS Applied Nano Materials, 2020, 3(9): 8875–8887
107. Song R, Cao X, Xu J, Zhou X, Wang X, Yuan N, Ding J O. N-codoped 3D graphene hollow sphere derived from metal-organic frameworks as oxygen reduction reaction electrocatalysts for Zn-air batteries. Nanoscale, 2021, 13(12): 6174–6183
108. Liu Y, Wang X, Zhao B, Shao X, Huang M. Fe/Fe_3C nanoparticles encapsulated in N-doped hollow carbon spheres as efficient electrocatalysts for the oxygen reduction reaction over a wide pH range. Chemistry, 2019, 25(41): 9650–9657
109. Wang Q, Lei Y, Chen Z, Wu N, Wang Y, Wang B, Wang Y. Fe/Fe_3C@C nanoparticles encapsulated in N-doped graphene-CNTs framework as an efficient bifunctional oxygen electrocatalyst for robust rechargeable Zn-air batteries. Journal of Materials Chemistry. A, Materials for Energy and Sustainability, 2018, 6(2): 516–526
110. Tan H, Li Y, Kim J, Takei T, Wang Z, Xu X, Wang J, Bando Y, Kang Y M, Tang J, et al. Sub-50 nm iron-nitrogen-doped hollow carbon sphere-encapsulated iron carbide nanoparticles as efficient oxygen reduction catalysts. Advancement of Science, 2018, 5(7): 1800120
111. Zhong Y, Xia X, Shi F, Zhan J, Tu J, Fan H J. Transition metal carbides and nitrides in energy storage and conversion. Advancement of Science, 2016, 3(5): 1500286
112. Li J S, Zhou Y W, Huang M J. Engineering Mo_xC nanoparticles confined in N, P-codoped porous carbon hollow spheres for enhanced hydrogen evolution reaction. Dalton Transactions (Cambridge, England), 2021, 50(2): 499–503
113. Chi J Q, Gao W K, Lin J H, Dong B, Yan K L, Qin J F, Liu B, Chai Y M, Liu C G N. P dual-doped hollow carbon spheres supported MoS_2 hybrid electrocatalyst for enhanced hydrogen evolution reaction. Catalysis Today, 2019, 330: 259–267
114. Cai Z S, Shi Y, Bao S S, Shen Y, Xia X H, Zheng L M. Bioinspired engineering of cobalt-phosphonate nanosheets for robust hydrogen evolution reaction. ACS Catalysis, 2018, 8(5): 3895–3902
115. Huang S, Meng Y, Cao Y, He S, Li X, Tong S, Wu M. N-, O- and P-doped hollow carbons: metal-free bifunctional electrocatalysts for hydrogen evolution and oxygen reduction reactions. Applied Catalysis B: Environmental, 2019, 248: 239–248
116. Zhao D, Sun K A, Cheong W C, Zheng L R, Zhang C, Liu S J, Cao X, Wu K L, Pan Y, Zhuang Z W, et al. Synergistically interactive pyridinic-N-MoP sites: identified active centers for enhanced hydrogen evolution in alkaline solution. Angewandte Chemie International Edition, 2020, 59(23): 8982–8990
117. Wang B, Wang Z, Wang X, Zheng B, Zhang W, Chen Y. Scalable synthesis of porous hollow $CoSe_2$-$MoSe_2$/carbon microspheres for highly efficient hydrogen evolution reaction in acidic and alkaline media. Journal of Materials Chemistry. A, Materials for Energy and Sustainability, 2018, 6(26): 12701–12707
118. Chen W, Qiao R, Song C, Zhao L, Jiang Z J, Maiyalagan T, Jiang Z. Tailoring the thickness of $MoSe_2$ layer of the hierarchical double-shelled N-doped carbon@$MoSe_2$ hollow nanoboxes for efficient and stable hydrogen evolution reaction. Journal of Catalysis, 2020, 381: 363–373
119. Wei Y, Zhang X, Zhao Z, Chen H S, Matras-Postolek K, Wang B, Yang P. Controllable synthesis of P-doped MoS_2 nanopetals decorated N-doped hollow carbon spheres towards enhanced hydrogen evolution. Electrochimica Acta, 2019, 297: 553–563
120. Yi M, Lu B, Zhang X, Tan Y, Zhu Z, Pan Z, Zhang J. Ionic liquid-assisted synthesis of nickel cobalt phosphide embedded in N, P codoped-carbon with hollow and folded structures for efficient hydrogen evolution reaction and supercapacitor. Applied Catalysis B: Environmental, 2021, 283: 119635
121. Wang F, Xiao L, Chen J, Chen L, Fang R, Li Y. Regulating the electronic structure and water adsorption capability by constructing carbon-doped CuO hollow spheres for efficient photocatalytic hydrogen evolution. ChemSusChem, 2020, 13(21): 5711–5721
122. Li Y, Zhang D, Fan J, Xiang Q. Highly crystalline carbon nitride hollow spheres with enhanced photocatalytic performance. Chinese Journal of Catalysis, 2021, 42(4): 627–636
123. Kang J, Byun S, Kim S, Lee J, Jung M, Hwang H, Kim T W, Song S H, Lee D. Design of three-dimensional hollow-sphere architecture of $Ti_3C_2T_x$ MXene with graphitic carbon nitride nanoshells for efficient photocatalytic hydrogen evolution. ACS Applied

Energy Materials, 2020, 3(9): 9226–9233
124. Zhang J W, Zhang H, Ren T Z, Yuan Z Y, Bandosz T J. FeNi doped porous carbon as an efficient catalyst for oxygen evolution reaction. Frontiers of Chemical Science and Engineering, 2021, 15(2): 279–287
125. Chen L, Ren J T, Wang Y S, Tian W W, Gao L J, Yuan Z Y. Organic-inorganic cobalt-phosphonate-derived hollow cobalt phosphate spherical hybrids for highly efficient oxygen evolution. ACS Sustainable Chemistry & Engineering, 2019, 7(15): 13559–13568
126. Dong Z, Zhang W, Xiao Y, Wang Y, Luan C, Qin C, Dong Y, Li M, Dai X, Zhang X. One-pot-synthesized cofe-glycerate hollow spheres with rich oxyhydroxides for efficient oxygen evolution reaction. ACS Sustainable Chemistry & Engineering, 2020, 8(14): 5464–5477
127. Li B Q, Zhao C X, Chen S, Liu J N, Chen X, Song L, Zhang Q. Framework-porphyrin-derived single-atom bifunctional oxygen electrocatalysts and their applications in Zn-air batteries. Advanced Materials, 2019, 31(19): 1900592
128. Sun X, Sun S, Gu S, Liang Z, Zhang J, Yang Y, Deng Z, Wei P, Peng J, Xu Y, et al. High-performance single atom bifunctional oxygen catalysts derived from ZIF-67 superstructures. Nano Energy, 2019, 61: 245–250
129. Zhang H, Liu Y, Chen T, Zhang J, Zhang J, Lou X W. Unveiling the activity origin of electrocatalytic oxygen evolution over isolated ni atoms supported on a N-doped carbon matrix. Advanced Materials, 2019, 31(48): 1904548
130. Tong J, Ma W, Bo L, Li T, Li W, Li Y, Zhang Q. Nitrogen-doped hollow carbon spheres as highly effective multifunctional electrocatalysts for fuel cells, Zn-air batteries, and water-splitting electrolyzers. Journal of Power Sources, 2019, 441: 227166
131. Sultan S, Tiwari J N, Singh A N, Zhumagali S, Ha M, Myung C W, Thangavel P, Kim K S. Single atoms and clusters based nanomaterials for hydrogen evolution, oxygen evolution reactions, and full water splitting. Advanced Energy Materials, 2019, 9(22): 1900624
132. Jin H, Wang J, Su D, Wei Z, Pang Z, Wang Y. *In situ* cobalt-cobalt oxide/N-doped carbon hybrids as superior bifunctional electrocatalysts for hydrogen and oxygen evolution. Journal of the American Chemical Society, 2015, 137(7): 2688–2694
133. Pu Z, Zhang C, Amiinu I S, Li W, Wu L, Mu S. General strategy for the synthesis of transition-metal phosphide/N-doped carbon frameworks for hydrogen and oxygen evolution. ACS Applied Materials & Interfaces, 2017, 9(19): 16187–16193
134. Tong J, Li Y, Bo L, Li W, Li T, Zhang Q, Kong D, Wang H, Li C. CoP/N-doped carbon hollow spheres anchored on electrospinning core–shell N-doped carbon nanofibers as efficient electrocatalysts for water splitting. ACS Sustainable Chemistry & Engineering, 2019, 7(20): 17432–17442
135. Dong Y, Zhou M, Tu W, Zhu E, Chen Y, Zhao Y, Liao S, Huang Y, Chen Q, Li Y. Hollow loofah-like N, O-Co-doped carbon tube for electrocatalysis of oxygen reduction. Advanced Functional Materials, 2019, 29(18): 1900015
136. Li J, Kang Y, Wei W, Li X, Lei Z, Liu P. Well-dispersed ultrafine CoFe nanoalloy decorated N-doped hollow carbon microspheres for rechargeable/flexible Zn-air batteries. Chemical Engineering Journal, 2021, 407: 127961
137. Chen S, Cheng J, Ma L, Zhou S, Xu X, Zhi C, Zhang W, Zhi L, Zapien J A. Light-weight 3D Co-N-doped hollow carbon spheres as efficient electrocatalysts for rechargeable zinc-air batteries. Nanoscale, 2018, 10(22): 10412–10419
138. Zhu X, Tan X, Wu K H, Chiang C L, Lin Y C, Lin Y G, Wang D W, Smith S, Lu X, Amal R N. P co-coordinated Fe species embedded in carbon hollow spheres for oxygen electrocatalysis. Journal of Materials Chemistry. A, Materials for Energy and Sustainability, 2019, 7(24): 14732–14742
139. Li Z, He H, Cao H, Sun S, Diao W, Gao D, Lu P, Zhang S, Guo Z, Li M, et al. Atomic Co/Ni dual sites and Co/Ni alloy nanoparticles in N-doped porous janus-like carbon frameworks for bifunctional oxygen electrocatalysis. Applied Catalysis B: Environmental, 2019, 240: 112–121
140. Jose V, Hu H, Edison E, Manalastas W Jr, Ren H, Kidkhunthod P, Sreejith S, Jayakumar A, Nsanzimana J M V, Srinivasan M, et al. Modulation of single atomic Co and Fe sites on hollow carbon nanospheres as oxygen electrodes for rechargeable Zn-air batteries. Small Methods, 2020, 5(2): 2000751
141. Wang J, Fan M, Tu W, Chen K, Shen Y, Zhang H. *In situ* growth of Co_3O_4 on nitrogen-doped hollow carbon nanospheres as air electrode for lithium-air batteries. Journal of Alloys and Compounds, 2019, 777: 944–953
142. Wu X, Niu Y, Feng B, Yu Y, Huang X, Zhong C, Hu W, Li C M. Mesoporous hollow nitrogen-doped carbon nanospheres with embedded $MnFe_2O_4$/Fe hybrid nanoparticles as efficient bifunctional oxygen electrocatalysts in alkaline media. ACS Applied Materials & Interfaces, 2018, 10(24): 20440–20447
143. Zhang D, Ma X, Zhang H, Liao Y, Xiang Q. Enhanced photocatalytic hydrogen evolution activity of carbon and nitrogen self-doped TiO_2 hollow sphere with the creation of oxygen vacancy and Ti^{3+}. Materials Today. Energy, 2018, 10: 132–140
144. Zheng Y, Liu Y, Guo X, Zhang W, Wang Y, Zhang M, Li R, Peng Z, Xie H, Huang Y S. Na co-doped graphitic carbon nitride/reduced graphene oxide hollow mesoporous spheres for photoelectrochemical catalysis application. ACS Applied Nano Materials, 2020, 3(8): 7982–7991
145. Shao B, Liu Z, Zeng G, Wu Z, Liu Y, Cheng M, Chen M, Liu Y, Zhang W, Feng H. Nitrogen-doped hollow mesoporous carbon spheres modified g-C_3N_4/Bi_2O_3 direct dual semiconductor photocatalytic system with enhanced antibiotics degradation under visible light. ACS Sustainable Chemistry & Engineering, 2018, 6(12): 16424–16436
146. Shao B, Liu X, Liu Z, Zeng G, Zhang W, Liang Q, Liu Y, He Q, Yuan X, Wang D, Luo S, Gong S. Synthesis and characterization of 2D/0D g-C_3N_4/CdS-nitrogen doped hollow carbon spheres (NHCs) composites with enhanced visible light photodegradation activity for antibiotic. Chemical Engineering Journal, 2019, 374: 479–493
147. Li X, Yan X, Hu X, Feng R, Zhou M, Wang L. Enhanced adsorption and catalytic peroxymonosulfate activation by metal-free N-doped carbon hollow spheres for water depollution. Journal of Colloid and Interface Science, 2021, 591: 184–192

148. Cheng C, Chen D, Li N, Xu Q, Li H, He J, Lu J. $ZnIn_2S_4$ grown on nitrogen-doped hollow carbon spheres: an advanced catalyst for Cr (VI) reduction. Journal of Hazardous Materials, 2020, 391: 122205
149. Zhang Y, Wang F, Ou P, Zhu H, Lai Y, Zhao Y, Shi W, Chen Z, Li S, Wang T. High efficiency and rapid degradation of bisphenol A by the synergy between adsorption and oxidization on the MnO_2@nano hollow carbon sphere. Journal of Hazardous Materials, 2018, 360: 223–232
150. Li X, Yan X, Hu X, Feng R, Zhou M, Wang L. Hollow Cu-Co/N-doped carbon spheres derived from ZIFs as an efficient catalyst for peroxymonosulfate activation. Chemical Engineering Journal, 2020, 397: 125533